

MATHEMATICAL MODELING OF VASCULAR STENTS*

J. TAMBAČA[†], M. KOSOR[‡], S. ČANIĆ[‡], AND D. PANIAGUA, M.D.[§]

Abstract. We present a mathematical model for a study of the mechanical properties of endovascular stents in their expanded state. The model is based on the theory of slender curved rods. Stent struts are modeled as linearly elastic curved rods that satisfy the kinematic and dynamic contact conditions at the “vertices” where the struts meet. This defines a stent as a mesh of curved rods. A weak formulation for the stent problem is defined and a finite element method for a numerical computation of its solution was developed. Numerical simulations showing the pressure-displacement (axial and radial) relationship for the entire stent are presented. From the numerical data and from the energy of the problem we deduced an “effective” pressure-displacement relationship of the law of Laplace-type for the mechanical behavior of stents, where the proportionality constant in the Laplace law was expressed explicitly in terms of the geometric and mechanic properties of a stent.

Key words. stents, mathematical modeling, theory of elasticity, curved rod model

AMS subject classifications. 74K10, 74K30, 74B05, 74S05

DOI. 10.1137/080722618

1. Introduction. A stent is a mesh tube that is inserted into a natural conduit of the body to prevent or counteract a disease-induced localized flow constriction. Endoluminal stents are used in the cardiovascular system (coronary arteries, pulmonary arteries, aorta, large systemic veins and arteries, etc.) as well as in the tracheobronchial, biliary, and urogenital systems. They play a crucial role in the treatment of coronary artery diseases (CAD). Coronary artery disease (or clogging, or *stenosis* of a coronary artery) is the major cause of heart attack, the leading cause of death in the United States. One person dies about every minute from a coronary event. Treatment of CAD entails inserting a catheter with a mounted balloon which is inflated to widen the lumen of a diseased artery (the area occupied by blood) and restore normal blood flow. This procedure is called balloon angioplasty. To prop the arteries open, a stent is inserted at the location of the narrowing. See Figure 1. Clinical and computational studies show that performance of coronary stents depends, among other things, on the geometrical properties of a stent, such as the number of stent struts, the strut width and thickness, and the geometry of the cross section of each stent strut, [21, 14, 6, 2, 12, 15, 11]. At the same time these geometric properties determine the overall mechanical properties of a stent.

By now, there is a large number of stents with different geometrical and mechanical features available on the market. Knowing the mechanical properties of a stent is

*Received by the editors April 28, 2008; accepted for publication (in revised form) November 16, 2009; published electronically February 19, 2010.

<http://www.siam.org/journals/siap/70-6/72261.html>

[†]Department of Mathematics, University of Zagreb, Bijenička 30, 10000 Zagreb, Croatia (tambaca@math.hr). Research supported in part by MZOS-Croatia under grant 037-0693014-2765 and by the NSF/NIH under grant DMS-0443826.

[‡]Department of Mathematics, University of Houston, Houston, 4800 Calhoun Road, Houston, TX 77204-3476 (mate.kosor@gmail.com, canic@math.uh.edu). The work of the second author was supported through NSF/NIH under grant DMS-0443826. The work of the third author was partially supported by the NSF under grant DMS-0337355, Texas Higher Education Board ARP 003652-0051-2006, NSF/NIH under grant DMS-0443826, and UH GEAR-2007 grant.

[§]Co-Director, Cardiac Catheterization Laboratories Michael E. DeBakey Veterans Medical Center, Assistant Professor of Medicine Baylor College of Medicine, St. Luke’s Episcopal Hospital/Texas Heart Institute, Houston, TX 77030-2604.

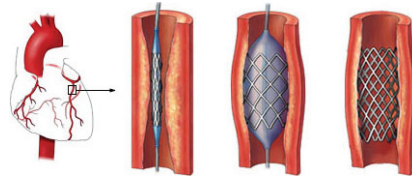


FIG. 1. *Deployment of a coronary stent.*

important in determining what pressure loads a stent can sustain when inserted in a native artery. Different medical applications require stents with different mechanical properties. As noted in [8], the therapeutic efficacy of stents depends exclusively on their mechanical properties.

Numerical studies of mechanical properties of vascular stents are a way to improve their design and performance. Even though a lot of attention has been devoted in cardiovascular literature to the use of endovascular prostheses over the past 10–15 years, the engineering and mathematical literature on the numerical studies of the mechanical properties of stents is not nearly as rich. Various issues in stent design and performance are important depending on the questions asked. They range from the study of large deformations that a stent undergoes during balloon expansion, for which nonlinear elasticity and plasticity need to be considered, all the way to the small deformations exhibited by an already expanded stent inserted in an artery, for which linear elasticity might be adequate. A range of issues has been studied in [5, 13] and the references therein, involving several different approaches. Most approaches, however, use commercial software packages based on the three-dimensional (3D) finite element method (FEM) structure approximations which may be computationally very expensive.

In this manuscript we present a *novel mathematical model* of a stent defined as a mesh of *one-dimensional curved rods*. A curved rod model is a one-dimensional (1D) approximation of a three-dimensional rod-like structure [9, 10]. In contrast with the beam theory which only takes into account transverse deformations of a beam in the direction of the force, the curved rod theory which was used in this manuscript to model the mechanical properties of stent struts takes into account deformations in all three spatial directions. This is particularly important in stent strut modeling in which, as shown in this manuscript, deformations in all three spatial directions take place and may be of the same order of magnitude, depending on the type of forcing. By prescribing the kinematic and dynamic contact conditions at the points where the curved struts meet (vertices), a stent is defined as a mesh of curved rods with the appropriate geometric properties.

Following a weak formulation of the stent problem as a mesh of 1D curved rods, we present the details of the development of a FEM approximation of the model equations in section 5. Our approach, based on the curved rod theory, simplifies the computation of the mechanical properties of stents depending on their geometric and mechanic parameters (in the realm of small deformations), thereby enabling a large number of simulations corresponding to different combinations of the geometric and mechanic parameters. (A comparison between a 3D and the 1D curved rod model performance is presented in Appendix B.)

We show numerical results indicating the overall, effective mechanical properties of stents depending on their geometric structure and on the struts' mechanical properties in section 6. We focus on a series of scenarios corresponding to an already

expanded stent undergoing small deformations due to a pressure load exerted to the interior and/or exterior stent surface. In particular, in section 7 we studied a relationship between the applied pressure and the displacement (radial and axial) as a function of the following parameters:

- Geometric parameters: t —thickness of stent struts, w —width of stent struts, n_O —number of vertices in the circumferential direction, $n_L + 1$ —number of vertices in the axial direction, R —stent reference radius (expanded), L —stent reference length (expanded).
- Mechanic parameters: E —struts Young’s modulus, μ —struts shear modulus.

This enabled us to generate a set of data that we used to deduce the overall, *effective* pressure-displacement relationship of the law of Laplace-type for the mechanical behavior of stents, where the proportionality constant in the Laplace law depends explicitly on the geometric and mechanic properties of a stent. Then, from the formulation of the stent problem as a minimization of an energy functional, obtained from its weak formulation, and by using simple geometric arguments, we were able to recover analytically the numerically derived effective pressure-displacement relationships.

The simple and elegant effective pressure-displacement formulas can be used, for example, to mimic stent compliancy in the more complex hemodynamics studies of fluid-structure interaction between blood flow and a stented artery, and, for example, to estimate the pressure load that a stent can sustain in the realm of small deformation (e.g., less than 10%), which is useful for manufacturing or choosing the right stent for a given application.

2. Stent frame geometry. During catheter deployment, high-precision laser cut stents are expanded using a balloon that has been premounted on a catheter. See Figure 1. In an expanded configuration the stent assumes a certain radius R and length L which will be called the *reference radius* and *reference length*, respectively. We are interested in describing the “stress-strain” relationship between the pressure load exerted on the outer and inner surfaces of a stent and the change in the diameter and length of a stent, for a given set of mechanical and geometrical stent parameters. Thus, we focus on the following problem: Given a set of parameters determining the geometric and mechanic properties of a stent, find the pressure-displacement relationship for the overall stent structure.

We consider a stent to be a three-dimensional elastic body defined as a union of three-dimensional struts (see Figures 2 and 3). The struts, which are three-dimensional, will be modeled by a *curved rod model*. A curved rod model is a one-dimensional approximation of a “thin” three-dimensional curved elastic structure given in terms of the arc-length of the middle curve of the rod as an unknown variable. The cross section of a rod representing each stent strut is assumed to be rectangular, of width w and thickness t . Thickness t is the dimension of a strut in the normal direction to the strut, as shown in Figure 4, which corresponds to the radial direction of the global cylindrical stent geometry. Struts themselves are assumed to be linearly elastic, with the elastic parameters given by the Lamé constants λ and μ , or, equivalently, by the Young’s modulus of elasticity E and the shear modulus μ .

Stent struts form a frame of diamonds with n_O vertices in the circumferential direction and $n_L + 1$ vertices in the longitudinal direction (see Figure 3). The presentation in this manuscript will focus on the uniform stent geometry, where all the struts are of equal length. This is, however, not required for the development of the theoretical and numerical methods described below, as they can be generalized to stents of arbitrary geometry with struts of different lengths. We have, in fact, used this fea-

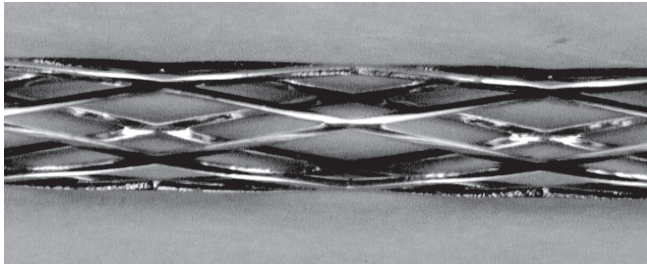


FIG. 2. A photograph of a stent with uniform geometry.

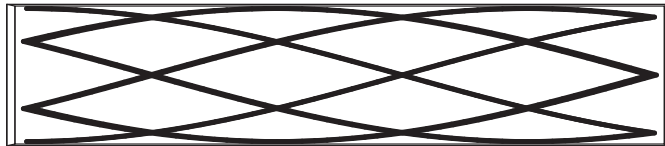


FIG. 3. A stent with $n_O = 6$ and $n_L = 5$.

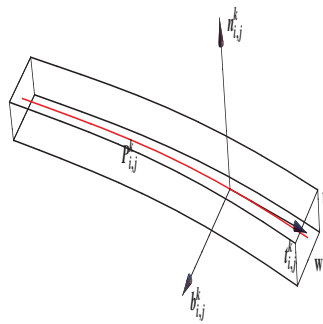


FIG. 4. A strut of width w and thickness t . The picture also shows the image of the middle curve parameterization $P_{i,j}^k$, and the local basis consisting of the tangent vector $t_{i,j}^k$, the normal vector $n_{i,j}^k$, and the bi-normal vector $b_{i,j}^k$, defined in (2.3). The normal vector $n_{i,j}^k$ corresponds to the radial direction in a stent.

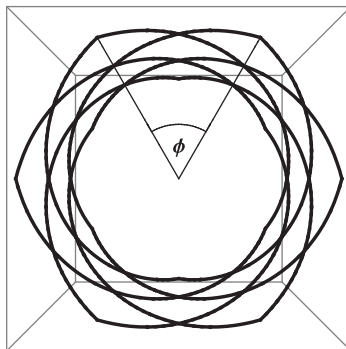


FIG. 5. The figure shows the angle formed by a vertex of a stent, the center of the circular cross section, and an adjacent vertex on the stent, denoted by $\phi = 2\pi/n_O$.

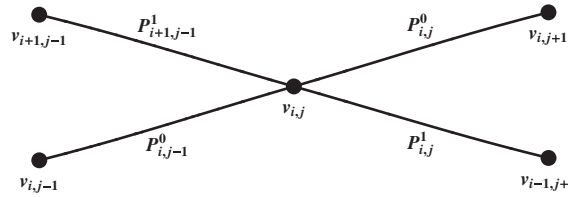


FIG. 6. The figure shows the nomenclature for the incoming and outgoing struts of the vertex $v_{i,j}$.

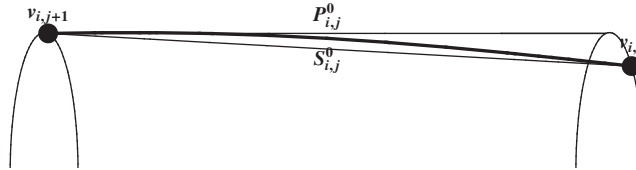


FIG. 7. Curved stent strut.

ture of our numerical method to test the mechanical properties of a nonuniform stent designed for a transcatheter implantation of an aortic valve prosthesis [16, 17, 20]. The presentation of the methods, however, is much clearer if we assume throughout this paper that our stent has a uniform geometry.

To describe the basic equations modeling the mechanical properties of stents, we introduce the following notation. Suppose that a transverse cross section of a stent is taken. Then the angle formed by a vertex of a stent, the center of the circular cross section, and an adjacent vertex on the same circumference of the stent, will be denoted by $\phi = 2\pi/n_O$. See Figure 5. The vertices on the adjacent circular cross section are shifted by the angle $\phi/2$. With this notation, the vertices on the stent can be described by

$$\mathbf{v}_{i,j} = \left(R \cos((i-1)\phi + (j-1)\phi/2), R \sin((i-1)\phi + (j-1)\phi/2), (j-1)\frac{L}{n_L} \right)^T,$$

where $j = 1, \dots, n_L + 1$ denotes the indices of the vertices in the longitudinal stent direction, and $i = 1, \dots, n_O$ denotes the indices of the vertices in the circumferential stent direction. Two incoming and two outgoing struts exist for all interior vertices. The incoming struts of a vertex $\mathbf{v}_{i,j}$ are those connecting the vertices shifted by the angle $\pm\phi/2$ at the level $j-1$ with the vertex $\mathbf{v}_{i,j}$. Similarly, the outgoing struts are those connecting the vertex $\mathbf{v}_{i,j}$ by the two vertices shifted by the angle $\pm\phi/2$ at the level $j+1$. See Figure 6.

Struts of a high-precision laser cut stainless steel stent are not straight, but curved and located on the cylinder of radius R . To write the equations for the curved stent struts we take a cord connecting the two vertices that define a strut, and then project the cord to the cylinder of radius R . See Figure 7. More precisely, denote by $R_{i,j}^k$, $k = 0, 1$, the two outgoing struts emerging from the vertex $\mathbf{v}_{i,j}$, and connecting to the vertices shifted by $\pm\phi/2$ at the level $j+1$. Then the cords (straight lines) connecting $\mathbf{v}_{i,j}$ to the vertices shifted by $\pm\phi/2$ at the level $j+1$ can be parameterized as

$$(2.1) \quad \begin{aligned} S_{i,j}^k(s) &= s\mathbf{v}_{i,j} + (1-s)\mathbf{v}_{((i-1-k) \bmod n_O)+1,j+1}, \quad s \in [0, 1], \\ i &= 1, \dots, n_O, \quad j = 1, \dots, n_L, \quad k = 0, 1, \end{aligned}$$

where $k = 0, 1$ corresponds to the struts $R_{i,j}^k$, $k = 0, 1$. The middle curve of the

curved stent struts $R_{i,j}^k$ can be expressed via the parameterization

$$P_{i,j}^k : [0, 1] \rightarrow \mathbb{R}^3$$

(see Figure 4), where

$$(2.2) \quad P_{i,j}^k(s) = NS_{i,j}^k(s), \quad s \in [0, 1], \quad i = 1, \dots, n_O, \quad j = 1, \dots, n_L, \quad k = 0, 1.$$

Here N is the operator that lifts the cord up to the cylinder of radius R :

$$N\mathbf{v} = P\mathbf{v} + R \frac{\mathbf{v} - P\mathbf{v}}{\|\mathbf{v} - P\mathbf{v}\|},$$

where P denotes the orthogonal projector on \mathbf{e}_3 in \mathbb{R}^3 with the standard scalar product, and $\{\mathbf{e}_1, \mathbf{e}_2, \mathbf{e}_3\}$ is the standard orthonormal basis of \mathbb{R}^3 .

The distance of the endpoints of a strut in \mathbb{R}^3 is given by

$$l_e = \sqrt{(R - R \cos(\phi/2))^2 + (R \sin(\phi/2))^2 + (L/n_L)^2}.$$

Note that this number is different from the strut length l_s but it is a good approximation of the strut length for the slightly curved struts.

We are now in a position to introduce a parameterization of the three-dimensional stent struts $R_{i,j}^k$ that define a three-dimensional stent Ω . Introduce a local basis at each point on the middle curve of strut $R_{i,j}^k$ (see Figure 4):

$$(2.3) \quad \mathbf{t}_{i,j}^k(s) = \frac{(P_{i,j}^k)'(s)}{\|(P_{i,j}^k)'(s)\|}, \quad \mathbf{n}_{i,j}^k(s) = \frac{(I - P)P_{i,j}^k(s)}{\|(I - P)P_{i,j}^k(s)\|}, \quad \mathbf{b}_{i,j}^k(s) = \mathbf{t}_{i,j}^k(s) \times \mathbf{n}_{i,j}^k(s)$$

for $s \in [0, 1]$. Then the three-dimensional strut $R_{i,j}^k$ can be parameterized by

$$\Phi_{i,j}^k(s_1, s_2, s_3) = P_{i,j}^k(s_1) + s_2 \mathbf{n}_{i,j}^k(s) + s_3 \mathbf{b}_{i,j}^k(s),$$

where $P_{i,j}^k$ is defined by (2.2). The parameterization $\Phi_{i,j}^k$ maps the set $[0, 1] \times [-t/2, t/2] \times [-w/2, w/2]$ into \mathbb{R}^3 . Notice that the normal vector points in the radial direction.

A stent Ω can now be defined as a three-dimensional domain which is a union of stent struts $R_{i,j}^k$ parameterized by $\Phi_{i,j}^k$:

$$(2.4) \quad \Omega = \cup_{i=1}^{n_O} \cup_{j=1}^{n_L} \cup_{k=0}^1 \Phi_{i,j}^k([0, 1] \times [-t/2, t/2] \times [-w/2, w/2]).$$

The *interior* stent surface of a stent is defined by

$$\Gamma_I = \cup_{i=1}^{n_O} \cup_{j=1}^{n_L} \cup_{k=0}^1 \Phi_{i,j}^k([0, 1] \times \{-t/2\} \times [-w/2, w/2]),$$

and the *exterior* stent surface by

$$\Gamma_E = \cup_{i=1}^{n_O} \cup_{j=1}^{n_L} \cup_{k=0}^1 \Phi_{i,j}^k([0, 1] \times \{t/2\} \times [-w/2, w/2]).$$

In this section we have described a geometry of the stent frame. This will be used in the following sections where we focus on modeling the mechanical properties of stents. In particular, we are interested in the mechanical response of an expanded stent Ω under the pressure load exerted on either the exterior surface Γ_E or the interior surface Γ_I . As we shall see later in this manuscript, we will be assuming small

deformations and small deformation gradients so that the theory of linear elasticity can be used to model a stent as a homogeneous, isotropic linearly elastic body by assuming that each stent strut satisfies the same mechanical properties. We will be interested in a *pure traction problem*. Namely, if a pressure load is applied to, e.g., the exterior surface of Ω , the remaining boundary will be assumed to be force free. A necessary condition for the existence of a solution to a pure traction problem is given by the requirement that the total force and the total moment applied to the structure be equal to zero (see, e.g., [4]). Moreover, the problem admits nonunique solutions: a solution is unique *up to* the infinitesimal rigid displacement $\mathbf{a} + \mathbf{b} \times x$, where $x \in \mathbb{R}^3$, and $\mathbf{a}, \mathbf{b} \in \mathbb{R}^3$ are arbitrary. Thus, in order to have a well-posed problem, we look for a function \mathbf{u} that is orthogonal in the L^2 -sense, to all infinitesimal rigid displacements, namely, such that

$$\int_{\Omega} \mathbf{u}(x) \cdot (\mathbf{a} + \mathbf{b} \times x) dx = 0 \quad \forall \mathbf{a}, \mathbf{b} \in \mathbb{R}^3.$$

These are the main ideas that will be followed in the subsequent sections. Additionally, to simplify analysis and numerical simulation of the entire stent structure, we approximate each three-dimensional “thin” stent strut by a *one-dimensional* curved rod model and use this approach to study the overall mechanical properties of a stent as a collection of one-dimensional curved rods. This approach is new in the study of mechanical properties of endovascular stents. It simplifies greatly numerical simulation of mechanical properties of stents, allowing complicated structures to be simulated in a very short time frame.

In the next section we describe the curved rod model for an approximation of a single stent strut and later define the appropriate boundary conditions at the points where the struts meet (vertices) to derive a mathematical model for the entire stent as a frame structure consisting of curved rods.

3. The curved rod model for a single stent strut. The curved rod model is a one-dimensional model that approximates a three-dimensional rod-like structure to the ϵ^2 accuracy, where ϵ is the ratio between the largest dimension of the cross section and the length of a rod. For a derivation and mathematical justification of the curved rod model see [9] and [10]. A numerical comparison between the performance of the one-dimensional curved rod model and a three-dimensional linearly elastic rod-like structure is presented in Appendix B. In general, the behavior of a three-dimensional rod-like elastic body is approximated by the behavior of its middle curve and of its cross sections. In the curved rod model, the cross sections behave approximately as infinitesimal rigid bodies that remain perpendicular to the deformed middle curve.

More precisely, let $P : [0, \ell] \rightarrow \mathbb{R}^3$ be the natural parameterization of the middle curve of the rod of length ℓ ($\|P'(s)\| = 1, s \in [0, \ell]$). Then the curved rod model can be formulated as a first-order system of differential equations for the following unknown functions:

- $\tilde{\mathbf{u}} : [0, \ell] \rightarrow \mathbb{R}^3$, the displacement of the middle curve of the rod;
- $\tilde{\boldsymbol{\omega}} : [0, \ell] \rightarrow \mathbb{R}^3$, the infinitesimal rotation of the cross section of the rod;
- $\tilde{\mathbf{q}} : [0, \ell] \rightarrow \mathbb{R}^3$, the contact moment; and
- $\tilde{\mathbf{p}} : [0, \ell] \rightarrow \mathbb{R}^3$, the contact force.

(Here ℓ corresponds to the strut length, denoted by l_s .) For a given line force density $\tilde{\mathbf{f}}$, the equations of the curved rod model can be written as (see [18])

$$(3.1) \quad \tilde{\mathbf{p}}' + \tilde{\mathbf{f}} = 0,$$

$$(3.2) \quad \tilde{\mathbf{q}}' + \mathbf{t} \times \tilde{\mathbf{p}} = 0,$$

describing the balance of contact force and contact moment, respectively, with

$$(3.3) \quad \tilde{\omega}' - \mathbf{QH}^{-1}\tilde{\mathbf{Q}}^T\tilde{\mathbf{q}} = 0,$$

$$(3.4) \quad \tilde{\mathbf{u}}' + \mathbf{t} \times \tilde{\omega} = 0,$$

describing the constitutive relations for a curved, linearly elastic rod. Here \mathbf{t} is the unit tangent to the middle curve, $\mathbf{Q} = (\mathbf{t}, \mathbf{n}, \mathbf{b})$ is the orthogonal matrix containing the tangent vector \mathbf{t} and vectors \mathbf{n} and \mathbf{b} that span the normal plane to the middle curve (\mathbf{Q} describes the local basis at each point of the middle curve), and

$$\mathbf{H} = \begin{bmatrix} \mu K & 0 & 0 \\ 0 & EI_b & 0 \\ 0 & 0 & EI_n \end{bmatrix},$$

where $E = \mu \frac{3\lambda+2\mu}{\lambda+\mu}$ is the Young's modulus of the material, I_n and I_b are moments of inertia of a cross section and μK is the torsion rigidity of the cross section. Therefore, \mathbf{H} describes the elastic properties of the rod and the geometry of the cross section. This model can also be obtained by a linearization of the Antman–Cosserat rod model (see [1]) under the material restriction of inextensibility and unshearability of a rod.

Equation (3.4) is a condition that requires that the middle line is approximately inextensible and that allowable deformations of the cross section are approximately orthogonal to the middle line. This condition has to be included in the solution space for the weak formulation of problem (3.1)–(3.4) (pure traction problem for a single curved rod). Thus, introduce the space

$$(3.5) \quad V = \{(\tilde{\mathbf{v}}, \tilde{\omega}) \in H^1(0, \ell)^6 : \tilde{\mathbf{v}}' + \mathbf{t} \times \tilde{\omega} = 0\}.$$

Function $(\tilde{\mathbf{u}}, \tilde{\omega}) \in V$ is called a weak solution of problem (3.1)–(3.4) if

$$(3.6) \quad \int_0^\ell \mathbf{QHQ}^T \tilde{\omega}' \cdot \tilde{\omega}' ds \\ = \int_0^\ell \tilde{\mathbf{f}} \cdot \tilde{\mathbf{v}} ds + \tilde{\mathbf{q}}(\ell) \cdot \tilde{\omega}(\ell) - \tilde{\mathbf{q}}(0) \cdot \tilde{\omega}(0) + \tilde{\mathbf{p}}(\ell) \cdot \tilde{\mathbf{v}}(\ell) - \tilde{\mathbf{p}}(0) \cdot \tilde{\mathbf{v}}(0)$$

holds for all $(\tilde{\mathbf{v}}, \tilde{\omega}) \in V$ (notice the difference in the notation between $\tilde{\omega}$ and $\tilde{\omega}$). Equation (3.6) will be used in the next section to define a weak formulation for the entire stent defined as a collection of curved rods. Boundary conditions appearing in (3.6) will be specified through the contact conditions at the stent vertices.

4. Stent as a collection of curved rods. We recall that in section 2 a stent Ω was defined as a three-dimensional domain which is a union of three-dimensional stent struts $R_{i,j}^k$ parameterized by $\Phi_{i,j}^k$; see (2.4). To model the mechanical behavior of a stent as a collection of *one-dimensional* linearly elastic, homogeneous, isotropic curved rods, we parameterize the struts using the one-dimensional parameterizations $P_{i,j}^k$ of the struts' middle curves; see (2.2). Now a stent can be defined as a union of *one-dimensional* parameterizations as follows:

$$F = \bigcup_{i=1}^{n_O} \bigcup_{j=1}^{n_L} \bigcup_{k=0}^1 P_{i,j}^k([0, 1]).$$

Note that parameterizations $P_{i,j}^k$ are not arc-length parameterizations which is necessary for the formulation of the curved rod model (3.1)–(3.4). Nevertheless, they

uniquely determine the middle curves of the stent struts and imply the existence of the arc-length parameterizations. Finding the arc-length parameterization in this case is a difficult task which, as we shall see later in section 4.1, is not necessary for the final formulation of the problem and the numerical method development.

Each of the curved rods approximating the stent struts $R_{i,j}^k$ satisfies a set of equations of the form (3.1)–(3.4); namely, for each $R_{i,j}^k$ we have

$$\begin{aligned}
 (\tilde{\mathbf{p}}_{i,j}^k)' + \tilde{\mathbf{f}}_{i,j}^k &= 0, \\
 (\tilde{\mathbf{q}}_{i,j}^k)' + \mathbf{t}_{i,j}^k \times \tilde{\mathbf{p}}_{i,j}^k &= 0, \\
 (\tilde{\boldsymbol{\omega}}_{i,j}^k)' - \mathbf{Q}_{i,j}^k \mathbf{H}^{-1} (\mathbf{Q}_{i,j}^k)^T \tilde{\mathbf{q}}_{i,j}^k &= 0, \\
 (\tilde{\mathbf{u}}_{i,j}^k)' + \mathbf{t}_{i,j}^k \times \tilde{\boldsymbol{\omega}}_{i,j}^k &= 0,
 \end{aligned}
 \tag{4.1}$$

on $\langle 0, l_s \rangle$; here $\mathbf{t}_{i,j}^k$ and $\mathbf{Q}_{i,j}^k$ denote the unit tangent vector function and the rotation matrix function for the curved rod $R_{i,j}^k$.

At the vertices where the curved rods meet, the kinematic and dynamic contact conditions determine the boundary condition for each curved rod in the stent frame structure. The kinematic contact condition describes the continuity of the kinematic quantities $\tilde{\mathbf{u}}_{i,j}^k$ and $\tilde{\boldsymbol{\omega}}_{i,j}^k$, stating that the displacement and the infinitesimal rotation for two struts meeting at a vertex are the same. The dynamic contact condition is the equilibrium condition requiring that the sum of all contact forces at a vertex and the sum of all contact moments at a vertex be equal to zero. Thus, for each vertex $\mathbf{v}_{i,j}$ the kinematic contact conditions are then given by

$$\tilde{\mathbf{u}}_{(i-1) \bmod n_O+1, j-1}^0(l_s) = \tilde{\mathbf{u}}_{i \bmod n_O+1, j-1}^1(l_s) = \tilde{\mathbf{u}}_{i,j}^0(0) = \tilde{\mathbf{u}}_{i,j}^1(0),
 \tag{4.2}$$

$$\tilde{\boldsymbol{\omega}}_{(i-1) \bmod n_O+1, j-1}^0(l_s) = \tilde{\boldsymbol{\omega}}_{i \bmod n_O+1, j-1}^1(l_s) = \tilde{\boldsymbol{\omega}}_{i,j}^0(0) = \tilde{\boldsymbol{\omega}}_{i,j}^1(0),
 \tag{4.3}$$

and the dynamic contact conditions are given by

$$\tilde{\mathbf{q}}_{(i-1) \bmod n_O+1, j-1}^0(l_s) + \tilde{\mathbf{q}}_{i \bmod n_O+1, j-1}^1(l_s) = \tilde{\mathbf{q}}_{i,j}^0(0) + \tilde{\mathbf{q}}_{i,j}^1(0),
 \tag{4.4}$$

$$\tilde{\mathbf{p}}_{(i-1) \bmod n_O+1, j-1}^0(l_s) + \tilde{\mathbf{p}}_{i \bmod n_O+1, j-1}^1(l_s) = \tilde{\mathbf{p}}_{i,j}^0(0) + \tilde{\mathbf{p}}_{i,j}^1(0),
 \tag{4.5}$$

for $i = 1, \dots, n_O, j = 1, \dots, n_L + 1$ with the convention that the quantity is removed for nonexistent indices corresponding to the end vertices $\mathbf{v}_{i,1}$ and \mathbf{v}_{i, n_L+1} .

To define a weak formulation for the stent frame problem, introduce the following function space:

$$V_F = \left\{ (\tilde{\mathbf{v}}_{1,1}^0, \tilde{\mathbf{w}}_{1,1}^0, \dots, \tilde{\mathbf{v}}_{n_O, n_L}^1, \tilde{\mathbf{w}}_{n_O, n_L}^1) : (\tilde{\mathbf{v}}_{i,j}^k, \tilde{\mathbf{w}}_{i,j}^k) \in V_{i,j}^k \ \& \ (4.2), (4.3) \text{ hold} \right\},$$

where $V_{i,j}^k$ are the function spaces (3.5) corresponding to the struts $R_{i,j}^k$.

Now the *weak formulation for the stent frame structure consisting of curved rods* is given by the following.

DEFINITION 4.1. *Function $(\tilde{\mathbf{u}}_{1,1}^0, \tilde{\boldsymbol{\omega}}_{1,1}^0, \dots, \tilde{\mathbf{u}}_{n_O, n_L}^1, \tilde{\boldsymbol{\omega}}_{n_O, n_L}^1) \in V_F$ is a weak solution to the stent frame problem (4.1)–(4.5) if*

$$\sum_{i=1}^{n_O} \sum_{j=1}^{n_L} \sum_{k=0,1} \int_0^{l_s} \mathbf{Q}_{i,j}^k \mathbf{H} (\mathbf{Q}_{i,j}^k)^T (\tilde{\boldsymbol{\omega}}_{i,j}^k)' \cdot (\tilde{\mathbf{w}}_{i,j}^k)' ds = \sum_{i=1}^{n_O} \sum_{j=1}^{n_L} \sum_{k=0,1} \int_0^{l_s} \tilde{\mathbf{f}}_{i,j}^k \cdot \tilde{\mathbf{v}}_{i,j}^k ds
 \tag{4.6}$$

holds for all $(\tilde{\mathbf{v}}_{1,1}^0, \tilde{\mathbf{w}}_{1,1}^0, \dots, \tilde{\mathbf{v}}_{n_O, n_L}^1, \tilde{\mathbf{w}}_{n_O, n_L}^1) \in V_F$.

Notice again the difference in the notation for the infinitesimal rotation test functions $\tilde{\mathbf{w}}_{i,j}^k$ and the notation for the infinitesimal rotation solution functions $\tilde{\omega}_{i,j}^k$. Also notice that all the intermediate boundary terms on the right-hand side of equation (3.6) cancel out in the formulation (4.6) due to the kinematic and dynamics contact conditions.

The solution to problem (4.6) is not unique. Namely, since only the derivative of $\tilde{\omega}$ appears in the weak formulation, the solution will be determined up to a constant $\tilde{\omega}_0$. Thus, if P is a point on the frame structure, then $\tilde{\omega}(P) = \tilde{\omega}_0$ is in the kernel of the problem. Furthermore, from the condition $\tilde{\mathbf{u}}' + \mathbf{t} \times \tilde{\omega} = 0$, with $\tilde{\omega}$ constant, one can solve the equation for $\tilde{\mathbf{u}}$ to obtain $\tilde{\mathbf{u}}(s) = \tilde{\mathbf{u}}_0 - P \times \tilde{\omega}_0 = \tilde{\mathbf{u}}_0 + \tilde{\omega}_0 \times P$. Thus, the infinitesimal rotation of the cross section and displacement of P are unique up to the term

$$\begin{bmatrix} \tilde{\omega}(P) \\ \tilde{\mathbf{u}}(P) \end{bmatrix} = \begin{bmatrix} \tilde{\omega}_0 \\ \tilde{\mathbf{u}}_0 + \tilde{\omega}_0 \times P \end{bmatrix},$$

for arbitrary vectors $\tilde{\mathbf{u}}_0, \tilde{\omega}_0 \in \mathbb{R}^3$. This means that the solution is unique up to the translation and infinitesimal rotation of the frame structure. Thus, as hinted earlier, we will be interested in the solution of (4.6) that satisfies an additional condition

$$(4.7) \quad \int_F \tilde{\mathbf{u}}(P) \cdot (\mathbf{a} + \mathbf{b} \times P) dP = 0 \quad \forall \mathbf{a}, \mathbf{b} \in \mathbb{R}^3.$$

The frame structure presented in this section is still extremely complex. The main obstacle for the numerical treatment of the problem of the form (4.6) is the implementation of the condition in the function spaces $V_{i,j}^k$ that should be satisfied by the test functions. For this reason, we make a further simplification that incorporates approximation of each curved rod by the piecewise straight rods. This approximation has been mathematically justified in [18] and [19].

4.1. Approximation of a curved rod by piecewise linear rods. Based on the results in [18] and [19], if we perturb the middle curve of a curved rod by δ in the $W^{1,\infty}$ -norm, the difference between the solution of the original problem $\mathbf{W} = (\tilde{\omega}, \tilde{\mathbf{u}})$ and the solution of the perturbed problem $\mathbf{W}^\delta = (\tilde{\omega}^\delta, \tilde{\mathbf{u}}^\delta)$ will satisfy the following estimate:

$$|\mathbf{W}(P) - \mathbf{W}^\delta(P)|_{L^\infty} \leq C\delta.$$

Thus, it is reasonable to introduce piecewise linear rods that approximate each curved rod in the following way. Consider the cords (straight line segments) $S_{i,j}^k$, defined in (2.1), connecting the two vertices defining a curved strut. Divide the cord $S_{i,j}^k$ into n_S equidistant segments, and “lift them up” to the cylindrical surface of radius R . These points define the new vertices

$$\begin{aligned} \mathbf{v}_{i,j}^{k,l} &= N \left(\frac{l}{n_S} \mathbf{v}_{i,j} + \left(1 - \frac{l}{n_S} \right) \mathbf{v}_{((i-1-k) \bmod n_O) + 1, j + 1} \right) = N S_{i,j}^k(l/n_S), \\ i &= 1, \dots, n_O, \quad j = 1, \dots, n_L, \quad k = 0, 1, \quad l = 1, \dots, n_S - 1. \end{aligned}$$

Connect the new vertices by straight line segments to define the new straight “struts” approximating the curved strut. Each new linear piece is of length $\ell_{i,j}^{k,l} = \|\mathbf{v}_{i,j}^{k,l} - \mathbf{v}_{i,j}^{k,l-1}\|$ and is parameterized by

$$\begin{aligned} P_{i,j}^{k,l}(s) &= \mathbf{v}_{i,j}^{k,l-1} + s \frac{\mathbf{v}_{i,j}^{k,l} - \mathbf{v}_{i,j}^{k,l-1}}{\|\mathbf{v}_{i,j}^{k,l} - \mathbf{v}_{i,j}^{k,l-1}\|}, \quad s \in [0, \ell_{i,j}^{k,l}], \quad i = 1, \dots, n_O, \\ j &= 1, \dots, n_L, \quad k = 0, 1, \quad l = 1, \dots, n_S, \end{aligned}$$

where the convention $\mathbf{v}_{i,j}^{k,0} = \mathbf{v}_{i,j}^k$ and $\mathbf{v}_{i,j}^{k,n_S} = \mathbf{v}_{((i-1-k) \bmod n_O)+1,j+1}$ is used. These parameterizations are natural; i.e., they are given in terms of the arc-length, as required by the curved rod model.

Now we use the fact that the formulation of the curved rod model (3.4) is valid for the piecewise smooth curves; see [18]. Each linear part can be treated as a straight rod with contact conditions of the same form as (4.2), (4.3) and (4.4), (4.5) at its ends, where there are only two struts intersecting at the new vertices. The weak formulation of this problem is of the same structure as that of problem (4.6), but with $2n_O n_L (n_S - 1)$ extra vertices.

Moreover, since all the rods are straight, the equations of equilibrium simplify. In particular, if we employ the following notation:

- u_t, u_n , and u_b are the tangential, normal, and binormal components of the local displacement, and
- τ is the tangential rotation of the cross section (torsion) [18],

then the last condition in (3.4) implies that $\tilde{\mathbf{u}}$ and $\tilde{\boldsymbol{\omega}}$ can be expressed as

$$\tilde{\mathbf{u}} = \mathbf{Q} \begin{bmatrix} u_t \\ u_n \\ u_b \end{bmatrix}, \quad \tilde{\boldsymbol{\omega}} = \mathbf{Q} \begin{bmatrix} \tau \\ -u'_b \\ u'_n \end{bmatrix}.$$

Moreover, for straight rods, condition (3.4) implies that u_t is constant, i.e., $u_t \in \mathbb{R}$. Thus, we no longer need to incorporate condition (3.4) in the function spaces $V_{i,j}^k$ which simplifies greatly the numerical implementation of the model equations.

The *weak formulation* for the problem in which each curved rod is approximated by *iecewise straight rods* now reads as follows.

Find $((u_{i,j}^{k,l})_t, (u_{i,j}^{k,l})_n, (u_{i,j}^{k,l})_b, \tau_{i,j}^{k,l}) \in \mathbb{R} \times H^2(0, \ell_{i,j}^{k,l}) \times H^2(0, \ell_{i,j}^{k,l}) \times H^1(0, \ell_{i,j}^{k,l})$ such that

$$\begin{aligned} & \sum_{i,j,k,l} \int_0^{\ell_{i,j}^{k,l}} EI_n (u_{i,j}^{k,l})''_n (v_{i,j}^{k,l})''_n + EI_b (u_{i,j}^{k,l})''_b (v_{i,j}^{k,l})''_b + \mu K (\tau_{i,j}^{k,l})' (\psi_{i,j}^{k,l})' ds \\ (4.8) \quad & = \sum_{i,j,k,l} \int_0^{\ell_{i,j}^{k,l}} (f_{i,j}^{k,l})_t (v_{i,j}^{k,l})_t + (f_{i,j}^{k,l})_n (v_{i,j}^{k,l})_n + (f_{i,j}^{k,l})_b (v_{i,j}^{k,l})_b ds \end{aligned}$$

holds for all $((v_{i,j}^{k,l})_t, (v_{i,j}^{k,l})_n, (v_{i,j}^{k,l})_b, \psi_{i,j}^{k,l}) \in \mathbb{R} \times H^2(0, \ell) \times H^2(0, \ell) \times H^1(0, \ell)$ satisfying the kinematic contact conditions at all the vertices, namely,

- at the original vertices determined by the curved rods:

$$\begin{aligned} \tilde{\mathbf{v}}_{i,j}^{0,1}(0) &= \tilde{\mathbf{v}}_{i,j}^{1,1}(0) = \tilde{\mathbf{v}}_{i \bmod n_O + 1, j - 1}^{1, n_S} \left(\ell_{i \bmod n_O + 1, j - 1}^{1, n_S} \right) \\ (4.9) \quad &= \tilde{\mathbf{v}}_{(i-1) \bmod n_O + 1, j - 1}^{0, n_S} \left(\ell_{(i-1) \bmod n_O + 1, j - 1}^{0, n_S} \right), \end{aligned}$$

$$\begin{aligned} \tilde{\boldsymbol{\omega}}_{i,j}^{0,1}(0) &= \tilde{\boldsymbol{\omega}}_{i,j}^{1,1}(0) = \tilde{\boldsymbol{\omega}}_{i \bmod n_O + 1, j - 1}^{1, n_S} \left(\ell_{i \bmod n_O + 1, j - 1}^{1, n_S} \right) \\ (4.10) \quad &= \tilde{\boldsymbol{\omega}}_{(i-1) \bmod n_O + 1, j - 1}^{0, n_S} \left(\ell_{(i-1) \bmod n_O + 1, j - 1}^{0, n_S} \right), \end{aligned}$$

for each $i = 1, \dots, n_O, j = 1, \dots, n_L$; and

- at the interior vertices determined by the piecewise linear rods:

$$(4.11) \quad \tilde{\mathbf{v}}_{i,j}^{0,l}(\ell_{i,j}^{0,l}) = \tilde{\mathbf{v}}_{i,j}^{0,l+1}(0), \quad \text{and} \quad \tilde{\boldsymbol{\omega}}_{i,j}^{0,l}(\ell_{i,j}^{0,l}) = \tilde{\boldsymbol{\omega}}_{i,j}^{0,l+1}(0),$$

for each $i = 1, \dots, n_O, j = 1, \dots, n_L$, and $l = 1, \dots, n_S - 1$.

Here

$$\tilde{\mathbf{f}}_{i,j}^{k,l} = \mathbf{Q} \begin{bmatrix} (f_{i,j}^{k,l})_t \\ (f_{i,j}^{k,l})_n \\ (f_{i,j}^{k,l})_b \end{bmatrix},$$

and E is the Young’s modulus, I_n and I_b are moments of inertia of a cross section, and μK is the torsion rigidity of a cross section, as defined in section 3.

5. The numerical method. To solve problem (4.8)–(4.11) we designed a numerical solver based on the finite element method. We solve problem (4.8)–(4.11) in terms of the displacement and rotation at the vertices. Denote them generically by $\tilde{\mathbf{U}} \in \mathbb{R}^3$ and $\tilde{\mathbf{W}} \in \mathbb{R}^3$. Recall that for each strut the displacement function $\tilde{\mathbf{u}}$ and rotation $\tilde{\boldsymbol{\omega}}$ are expressed by u_t, u_n, u_b , and τ . We approximate these functions by the following polynomials:

$$\begin{aligned} u_t(s) &= E_t, & u_n(s) &= B_n s^3 + C_n s^2 + D_n s + E_n, \\ u_b(s) &= B_b s^3 + C_b s^2 + D_b s + E_b, & \tau(s) &= 2C_t s + D_t. \end{aligned}$$

These polynomials satisfy $u'_t = 0$, i.e., $u_t \in \mathbb{R}$, and $(u_n, u_b, \psi) \in H^2(0, \ell) \times H^2(0, \ell) \times H^1(0, \ell)$, for an appropriate segment length ℓ .

Let $\tilde{\mathbf{U}}_0, \tilde{\mathbf{W}}_0, \tilde{\mathbf{U}}_\ell, \tilde{\mathbf{W}}_\ell$ denote the displacement and rotation of the cross section at the endpoints of each given linear piece. Then, for each $\tilde{\mathbf{U}}_0, \tilde{\mathbf{W}}_0, \tilde{\mathbf{U}}_\ell, \tilde{\mathbf{W}}_\ell$ we are able to express v_t, v_n, v_b , and ψ uniquely under the condition that

$$(5.1) \quad \tilde{\mathbf{U}}_0 \cdot \mathbf{t} = u_t(0) = u_t(\ell) = \tilde{\mathbf{U}}_\ell \cdot \mathbf{t}.$$

This condition is a consequence of the fact that for straight rods $(u_t)' = 0$. This condition should be satisfied by both the unknown functions (solution) and the test functions for all linear pieces. To enforce this condition, we employ the approach based on the Lagrange multipliers. The final linear system is of the form

$$(5.2) \quad \begin{bmatrix} \mathbf{A} & \mathbf{C}^T \\ \mathbf{C} & \mathbf{0} \end{bmatrix} \begin{bmatrix} \mathbf{X} \\ \mathbf{Y} \end{bmatrix} = \begin{bmatrix} \mathbf{F} \\ \mathbf{0} \end{bmatrix},$$

where \mathbf{X} is a vector of unknown functions $\mathbf{X} = (\tilde{\mathbf{U}}_1, \tilde{\mathbf{W}}_1, \dots, \tilde{\mathbf{U}}_{n_v}, \tilde{\mathbf{W}}_{n_v})^T$, with $n_v = n_O(n_L + 1) + 2n_{ONL}(n_S - 1)$ denoting the number of all vertices and \mathbf{Y} the vector of Lagrange multipliers. The dimension of \mathbf{X} is equal to six times the number of all vertices n_v , and the dimension of \mathbf{Y} is equal to the total number of all linear struts $2n_{ONL}n_S$. The matrix \mathbf{A} is the stiffness matrix of the system which is symmetric. \mathbf{C} is the matrix of conditions (5.1).

The solution of problem (4.8)–(4.11) is not unique. The matrix of the system (5.2) is singular with the kernel of dimension 6. As mentioned earlier, to obtain a unique solution, we seek a solution which satisfies the additional condition (4.7). A discrete form of this condition can be written as

$$\sum_{i,j,k} \tilde{\mathbf{U}}_{i,j}^{k,l} = \sum_{i,j,k} \tilde{\mathbf{W}}_{i,j}^{k,l} = 0.$$

To enforce condition (4.7) we use the penalization method.

A code written in C++ was developed to implement this approach. We have been working with frames consisting of 100–250 vertices, so the matrices of the systems are of dimensions up to 2000. The time to solve the problem numerically varies from 0.3 to 5 seconds on a server with one Intel Xeon 3.00 GHz processor and 2GB of RAM.

6. Numerical results. In most of the examples below, various configurations of stents will be exposed to the exterior pressure loads of 0.5 atmospheres. This pressure load is physiologically reasonable since stents are typically oversized by 10% of the native vessel radius to provide reasonable fixation. If we assume an approximate Young's modulus of a coronary artery to be between 10^5Pa and 10^6Pa (see [3]), then using the law of Laplace one can estimate an approximate pressure exerted by the arterial wall to a coronary stent to be around 0.5 atm.

A series of examples below will investigate how stents respond to uniform versus nonuniform pressure loads, and how their overall mechanical properties depend on the stent geometry and structure. These examples will serve as a motivation to derive an overall stress-strain relationship (pressure-displacement) of the "Law of Laplace"-type in terms of the geometric parameters of the stent, presented in section 7. We note here that although the magnitude of the global radial or longitudinal displacement of the entire stent in these examples may be greater than 10%, the maximal displacement of the stent struts is considerably smaller. This is discussed in Appendix A.

In the first two examples we show that the magnitudes of the radial and longitudinal displacement of a stent under a uniform pressure load are larger if the stent is not maximally expanded. Stents that are expanded to a larger radius are stiffer. Thus, in endovascular procedures in which stents are deployed to the regions exhibiting very high pressure loads such as, for example, the annuli of the aortic heart valves in the aortic valve replacement, balloon expansion of the annular stent should be performed in a way that would ensure maximal stent expansion.

Example 6.1. A stainless steel stent (316L) with 8 vertices in the circumferential direction and 7 vertices in the longitudinal (axial) direction is considered. The length of each strut is 6mm. The stent has been expanded to the radius of 1cm into its reference configuration. The stent is subject to a uniform pressure load of 0.5 atmosphere applied to the exterior wall. As a result, the stent deforms and exhibits both the axial and longitudinal displacement. The maximum radial displacement is assumed at the endpoints of the stent, and it is equal to 1.52656mm (15% of the reference configuration). Figures 8, 9, and 10 show the magnitude of the radial and axial displacement, the total displacement and magnitude of rotation of cross section, and contact moment and contact force, respectively. Negative displacement in Figure 8 corresponds to compression, while positive displacement corresponds to expansion. Notice that the maximum radial and longitudinal displacements occur at the endpoints of a stent, and that the largest cross-section rotation occurs at the middle of the strut with the maximum cross-section rotation occurring for the end struts. Additionally, Figure 10 left shows that the largest contact moments occur at the stent's vertices with the maximal contact moments occurring at the end vertices. Figure 10 right shows that the maximal contact force occurs at the end struts of a stent.

Example 6.2. All the stent parameters in this example as well as the magnitude of the pressure load are the same as those in Example 6.1. The only difference is the reference configuration to which the stent has been expanded: The stent is now expanded to 0.8 of the reference configuration in the previous example, i.e., to 8mm. Our results below show that the maximal radial displacement is now 1.88614mm which is 23.5% of the reference configuration. This is in contrast with the 15.2% corresponding to the maximal radial displacement in Example 6.1. Thus, we conjecture that the larger the expansion of a stent, the larger the pressure loads that can be supported by the stent. See Figure 11.

The next two examples show that nonuniform pressure loads cause higher stent deformations. This corresponds to, for example, a situation when a stent is inserted in

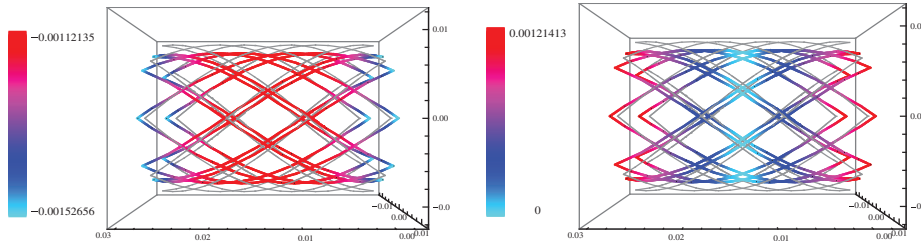


FIG. 8. The magnitude of the radial (left) and axial (right) displacement for a stent in Example 6.1.

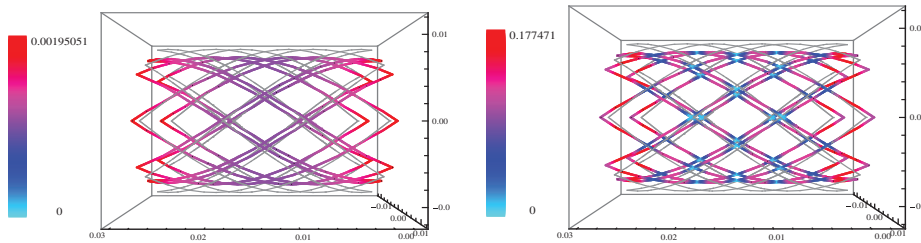


FIG. 9. The magnitude of the total displacement (left) and rotation (right) of cross sections for a stent in Example 6.1.

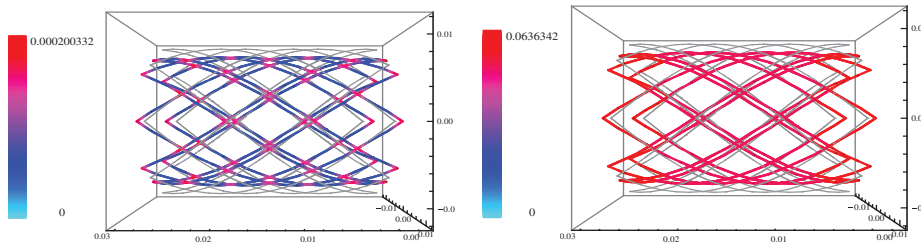


FIG. 10. The magnitude of the contact moment (left) and the contact force (right) for a stent in Example 6.1.

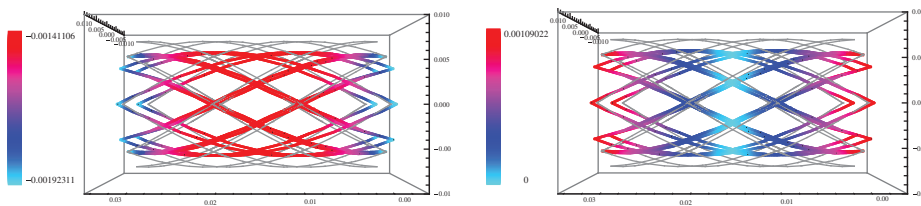


FIG. 11. The magnitude of the radial (left) and axial (right) displacement for a stent in Example 6.2.

a vessel lumen with either high diameter gradients or nonaxially symmetric geometry which can occur due to, for example, plaque deposits that have not been uniformly pushed against the wall of a diseased artery during balloon angioplasty. We will show that in this case the global stiffness of a stent is smaller than that of a stent under uniform pressure loads. Thus, a stent deployed to the lumen of an artery whose

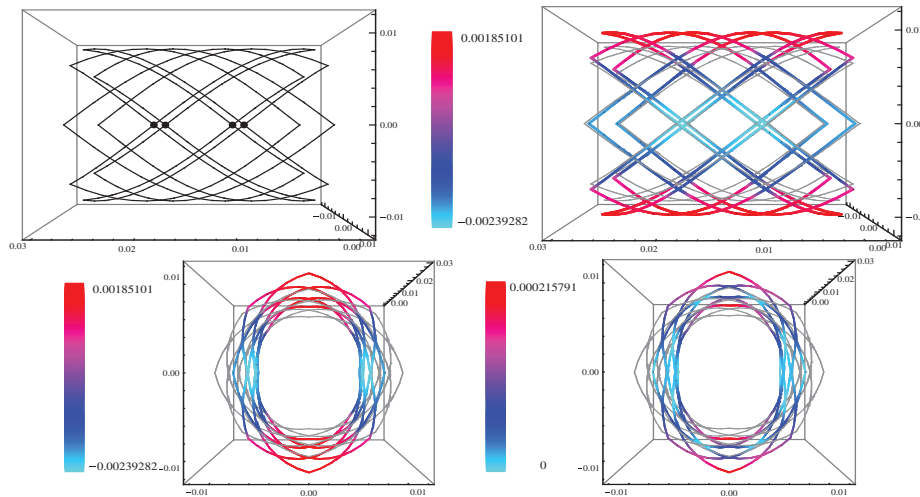


FIG. 12. The top figure on the left shows the four points at which the pressure load is applied to the stent described in Example 6.3. The remaining three figures show the deformation of the stent superimposed over the reference configuration shown in grey. The stent struts are colored based on the magnitude of the radial displacement.

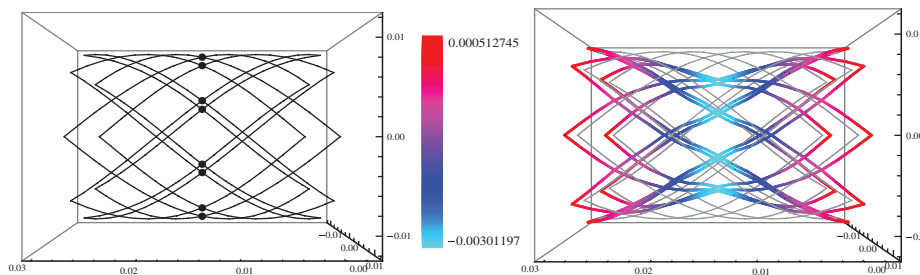


FIG. 13. The figure on the left shows the eight points at which the pressure load is applied to the stent described in Example 6.4. The figure on the right shows the deformation of the stent superimposed over the reference configuration shown in grey. The stent struts are colored based on the magnitude of the radial displacement.

diameter exhibits high gradients will deform more than a stent deployed in an artery with nearly constant diameter and axially symmetric geometry.

Example 6.3. A stent from Example 6.1 is considered with the reference radius of 1cm. A total load, which corresponds to the total forcing of uniform pressure of 0.05 atmosphere, is applied to the four points shown in Figure 12. Our numerical simulations, presented in Figure 12, show that the maximal radial displacement equals 2.39282mm, which is almost two times the displacement achieved at the ten times greater forcing applied uniformly. Additionally, the deformation, as expected, is nonuniform: The stent is compressed in the direction of the applied force and expanded in the direction perpendicular to the applied force.

Example 6.4. A stent from Example 6.1 is considered with the reference radius of 1cm. A force is applied to the eight points in the middle of the stent, shown in Figure 13. The force applied at each of the eight points is equal to 1/8 of the total force that corresponds to the uniform pressure load of 0.5 atm. The absolute value

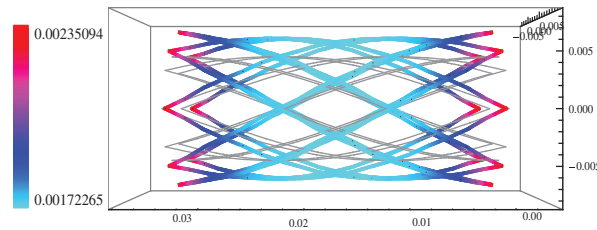


FIG. 14. A stent from Example 6.1 is exposed to the uniform pressure of 0.5 atm applied to the interior surface of the stent. The figure shows the dogboning effect (flaring of the proximal and distal ends of a stent) typically observed during balloon expansion of a stent. See Example 6.5.

of the calculated maximal radial displacement is equal to $3.01197 \times 10^{-3}m$ which is about two times the maximal radial displacement from Example 6.1.

Example 6.5. The stent from Example 6.1 with the reference radius of $R = 0.5cm$ is exposed to the uniform pressure of 0.5 atm applied to the interior surface of the stent. Figure 14 shows that our model captures the “dogboning” effect corresponding to the flaring of the proximal and distal ends of a stent, observed during balloon expansion of the stent.

In the last sequence of six examples we study how the pressure-displacement relationship for a given, uniform stent depends on the following geometric and mechanic properties of a stent: the Young’s modulus E , the shear modulus μ , the thickness of each stent strut t , the width of each stent strut w , the stent reference radius R , and the stent reference length L . In all of those examples the stent is subject to a uniform pressure load of 0.5 atmospheres applied to the exterior surface of the stent. We begin with Example 6.6 which will serve as a benchmark against which the results from Examples 6.7 through 6.12 will be compared.

Example 6.6. In this example we begin with a stent with the parameter values shown in Table 1. The stent is subject to a uniform pressure load of 0.5 atmospheres applied to the exterior surface of the stent. Figure 15 shows the deformation of the stent with the colors of the struts corresponding to the magnitude of the total displacement. The calculated radial displacement at the middle vertex of the stent is equal to $3.35 \times 10^{-4}m$.

In the next two examples we vary the Young’s modulus E and the shear modulus μ independently to see how the displacement of a stent is influenced by those two parameters independently. The choice of the two parameters was motivated by the fact that they appear in the coefficients of the curved rod model. Even though in an isotropic material, the Young’s modulus and the shear modulus are linked by $\mu = E/2 * (1 + \nu)$, the main purpose of the two numerical tests presented in Examples 6.7

TABLE 1
Parameter values for a stent in Example 6.6.

n_O	Number of vertices in circumferential direction	8
$n_L + 1$	Number of vertices in axial direction	7
E	Young’s modulus of elasticity	$2.1 \times 10^{11}Pa$
μ	Shear modulus	$8.3 \times 10^{10}Pa$
t	Thickness of each strut	0.0001 m
w	Width of each strut	0.0001 m
R	Stent reference radius	0.01 m
L	Stent reference length	0.018 m

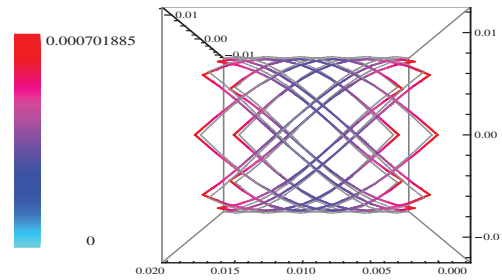


FIG. 15. Stent from Example 6.6. The stent struts are colored based on the magnitude of total displacement. The reference configuration is shown in grey.

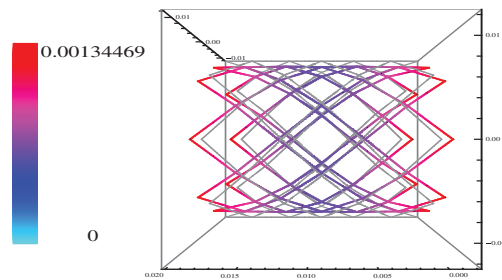


FIG. 16. Stent from Example 6.7. The stent struts are colored based on the magnitude of total displacement. The reference configuration is shown in grey.

and 6.8 was to show the *poor influence of the torsion*. This is later confirmed in the derivation of the effective pressure-displacement relationship in section 7.

Example 6.7. Consider a stent with the parameter values from Table 1, except for the Young's modulus which is now taken to be one-half of the Young's modulus from Table 1, i.e., $E = 1.05 \times 10^{11}$ Pa. Under the applied uniform pressure of 0.5 atmospheres, our simulation provides the radial displacement at the middle vertex of the stent equal to 6.65×10^{-4} m which is around twice the size of the radial displacement from the previous case. The corresponding deformed stent is shown in Figure 16.

Example 6.8. Consider a stent with the parameter values from Table 1 except for the shear modulus which is now taken to be half of the shear modulus from Table 1, i.e., $\mu = 4.15 \times 10^{10}$ Pa. The stent is subject to the uniform pressure load of 0.5 atmospheres. Our simulation provides the radial displacement at the middle vertex of the stent equal to 3.38×10^{-4} m, which is almost the same as the radial displacement in Example 6.6. The corresponding deformed stent is shown in Figure 17. Thus, changing the shear modulus μ does not seem to influence the stent displacement to the leading order.

Example 6.9. Consider a stent with the parameter values from Table 1 except for the thickness of each strut which is now taken to be half of the thickness from Table 1, i.e., $t = 0.00005$ m. The stent is subject to the uniform pressure load of 0.5 atmospheres. Our simulation provides the radial displacement at the middle vertex of the stent equal to 6.96×10^{-4} m, which is double the radial displacement from Example 6.6. The corresponding deformed stent is shown in Figure 18.

Example 6.10. Consider a stent with parameter values from Table 1 except for the width of each strut which is now taken to be half of the width from Table 1, i.e., $w = 0.00005$ m. The stent is subject to the uniform pressure load of 0.5 atmospheres.

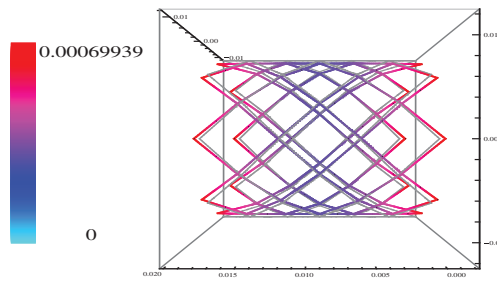


FIG. 17. Stent from Example 6.8. The stent struts are colored based on the magnitude of total displacement. The reference configuration is shown in grey.

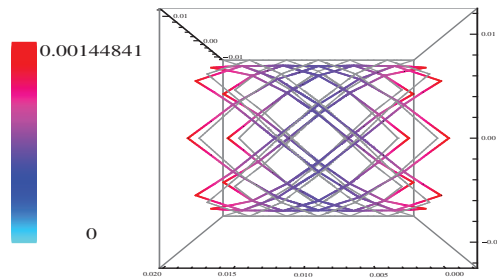


FIG. 18. Stent from Example 6.9. The stent struts are colored based on the magnitude of total displacement. The reference configuration is shown in grey.

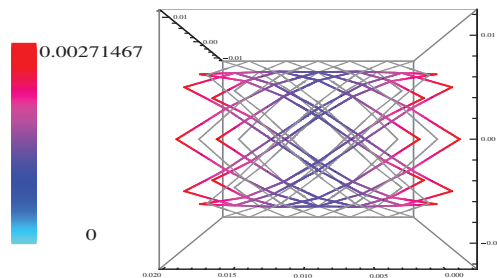


FIG. 19. Stent from Example 6.10. The stent struts are colored based on the magnitude of total displacement. The reference configuration is shown in grey.

Our simulation provides the radial displacement at the middle vertex of the stent equal to $1.28 \times 10^{-3}m$, which is four times the radial displacement from Example 6.6. The corresponding deformed stent is shown in Figure 19.

Example 6.11. Consider a stent with parameter values from Table 1 except for the reference total length of the stent which is now taken to be half of the reference length from Table 1, i.e., $L = 0.09m$. This means, in particular, that the total length of the struts is now smaller than the total strut length for a stent with parameters described in Table 1. All the other parameters are the same as those presented in Table 1. The stent is subject to the uniform pressure load of 0.5 atmospheres. Our simulation provides the radial displacement at the middle vertex of the stent equal to $6.34 \times 10^{-5}m$ which is smaller than the radial displacement of the stent with reference length from Table 1. Thus, shorter stents with the same number of vertices are stiffer than longer stents. The corresponding deformed stent is shown in Figure 20.

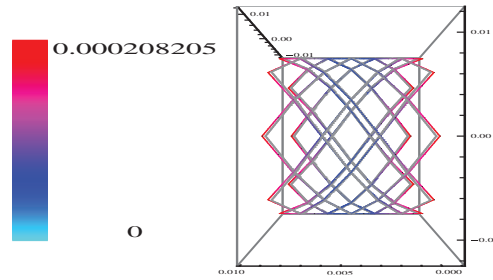


FIG. 20. Stent from Example 6.11. The stent struts are colored based on the magnitude of the total displacement. The reference configuration is shown in grey.

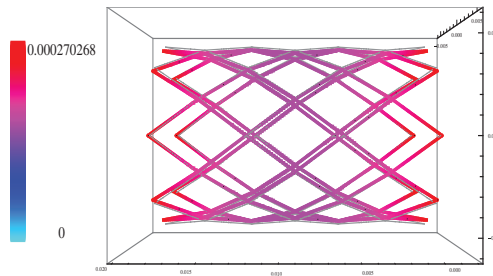


FIG. 21. Stent from Example 6.12. The stent struts are colored based on the magnitude of total displacement. The reference configuration is shown in grey.

Example 6.12. Consider a stent with parameter values from Table 1 except for the reference radius of the stent which is now taken to be half of the reference radius from Table 1, i.e., $R = 0.005\text{m}$. Again, this means, in particular, that the total length of stent struts is smaller than the total length of the stent struts from Example 6.6. All the other parameters are the same as those in Table 1. The stent is subject to the uniform pressure load of 0.5 atmospheres. Our simulation provides the radial displacement at the middle vertex of the stent equal to $1.74 \times 10^{-4}\text{m}$ which is about half the radial displacement of the stent from Example 6.6. Thus, the smaller the reference radius of a stent, the stiffer the stent. The corresponding deformed stent is shown in Figure 21.

7. An effective model for the global behavior of a uniform stent. The goal of this section is to derive a simple model, in the form of the Laplace law, for the global behavior of the entire stent. In particular, we are interested in deriving a relationship between the applied uniform pressure and the following displacements: (1) the radial displacement at the middle of a stent, (2) the longitudinal displacement at the endpoints of a stent.

Recall that Laplace law for a linearly elastic membrane reads [7]

$$p = \frac{Et}{(1 - \sigma^2)R^2}u.$$

For small deformations and small deformation gradients, we aim at describing the global behavior of a stent by looking for a relationship of the same form

$$p = Ku,$$

where p is the applied uniform pressure, u is the stent displacement (radial or longitudinal), and K is the proportionality constant that depends on the following parameters:

- material properties described by E, μ ;
- geometry of the strut cross section described by w, t ; and
- overall geometry of the stent described by R, L, n_O , and n_L .

Thus, the aim is to identify the constant K in terms of the mechanic and geometric parameters of the stent. We will first obtain an expression for K by combining the finite element method-based numerical experiments and the least square approximation of the experimental data and then derive the same formula using the minimization (of energy) formulation of the stent problem and a simple geometric argument.

We begin by assuming the following homogeneous dependence of K on the parameters in the problem:

$$(7.1) \quad p = kE^{\alpha_1} \mu^{\alpha_2} w^{\alpha_3} t^{\alpha_4} R^{\alpha_5} L^{\alpha_6} u,$$

where we need to identify the powers α_i and the constant k , where $k = k(n_O, n_L)$ will embody the dependence of the pressure-displacement relationship on the geometrical parameters n_O and n_L . As we shall see below, our numerical investigation leading to the values of the powers α_i produced amazing results implying integer values of the powers α_i that provide excellent agreement with the (numerical) experiments and with the effective equations derived from the energy equality.

To determine the powers α_i we first rewrite the problem in linear form by taking the logarithm of (7.1) to obtain

$$(7.2) \quad \log p = \log k + \alpha_1 \log E + \alpha_2 \log \mu + \alpha_3 \log w + \alpha_4 \log t + \alpha_5 \log R + \alpha_6 \log L + \log u.$$

We then use the linear least square method to approximate the data obtained using the finite element method, described in the previous section. We ran the finite element method on the following set of parameters:

$$\begin{aligned} E &\in 2.1 \times 10^{11} \times \{0.8, 0.85, 0.9, 0.95, 1, 1.05, 1.1, 1.15, 1.2\} \text{Pa}, \\ \mu &\in 8.31 \times 10^{10} \times \{0.85, 0.9, 0.95, 1, 1.05, 1.1, 1.15\} \text{Pa}, \\ w &\in 0.0001 \times \{0.5, 0.6, 0.7, 0.8, 0.9, 1, 1.1, 1.2, 1.3, 1.4, 1.5\} \text{m}, \\ t &\in 0.0001 \times \{0.5, 0.6, 0.7, 0.8, 0.9, 1, 1.1, 1.2, 1.3, 1.4, 1.5\} \text{m}, \\ R &\in 0.01 \times \{0.6, 0.65, 0.7, 0.75, 0.8, 0.85, 0.9, 0.95, 1, 1.05, 1.1, 1.15, 1.2\} \text{m}, \\ L &\in 0.018 \times \{0.8, 0.9, 1, 1.1, 1.2, 1.3, 1.4, 1.5\} \text{m}. \end{aligned}$$

For each set of values of $\{E, \mu, w, t, R, L\}$ and a given, fixed, pressure p , the corresponding displacement was recovered by the finite element method. The linear least square method is then used to approximate the obtained numerical results using a function of the form (7.2). For the pressure-longitudinal displacement relationship the results of the least square method are shown in Table 2. For the pressure-radial displacement relationship the results of the least square method are shown in Table 3.

CONCLUSION 1. *The least square method suggests the following values of α_i :*

$$\alpha_1 = 1, \quad \alpha_2 = 0, \quad \alpha_3 = 2, \quad \alpha_4 = 1.$$

Notice that $\alpha_2 = 0$ confirms the poor influence of the torsion, as suggested by Examples 6.7 and 6.8 in section 5.

TABLE 2
Parameters for the pressure-longitudinal displacement relationship.

	$\log k_l$	α_1	α_2	α_3	α_4	α_5	α_6
$n_O = 6, n_L = 6$	-4.114	0.990	0.009	1.973	1.030	-2.260	-1.694
$n_O = 8, n_L = 6$	-3.868	0.995	0.004	1.983	1.019	-1.995	-1.955
$n_O = 12, n_L = 6$	-3.600	0.998	0.001	1.992	1.009	-1.631	-2.324

TABLE 3
Parameters for the pressure-radial displacement relationship.

	$\log k_r$	α_1	α_2	α_3	α_4	α_5	α_6
$n_O = 6, n_L = 6$	-3.439	0.987	0.012	1.940	1.053	-1.275	-2.678
$n_O = 8, n_L = 6$	-3.419	0.991	0.008	1.950	1.047	-1.005	-2.945
$n_O = 12, n_L = 6$	-3.484	0.997	0.002	1.978	1.024	-0.634	-3.321

TABLE 4
Value of parameters in formula (7.3) with u corresponding to the longitudinal displacement

	$\log k_l$	α_1	α_2	α_3	α_4	α_5	α_6
$n_O = 6, n_L = 6$	-1.252	0.990	0.009	3.973	1.030	-1.012	-0.988
$n_O = 8, n_L = 6$	-0.997	0.995	0.004	3.983	1.019	-1.006	-0.993
$n_O = 12, n_L = 6$	-0.643	0.998	0.001	3.992	1.009	-1.002	-0.997

To fix the last two powers, we rescale the pressure by the square of the approximate cross-sectional area. This is the total area of the stent material, assuming a linear approximation of the curved stent struts (using l_e instead of l_s). The total area is given by

$$A = 2n_L n_O w l_e.$$

This proved to be the correct approach, since, as we shall see below, this produced the values of new parameters α_5 and α_6 independent of n_O . Thus, we reformulate the problem by looking for the pressure-displacement relationship of the form

$$(7.3) \quad p = \frac{k}{A^2} E^{\alpha_1} \mu^{\alpha_2} w^{\alpha_3} t^{\alpha_4} R^{\alpha_5} L^{\alpha_6} u, \quad A = 2n_L n_O w l_e.$$

The least square method was then run for the approximation of the form (7.3), and the relative ℓ^2 error between the FEM simulation and formula (7.3) was calculated based on the following formula:

$$\text{Error} = \frac{1}{N} \sum_{\text{Data Set}} \left(\frac{\text{FEM simulation} - \text{result using (7.3)}}{\text{result using (7.3)}} \right)^2,$$

where N is the number of points in Data Set. Table 4 shows the results obtained using the least square method.

Based on these results we conclude the following.

CONCLUSION 2. The assumption (7.3) on the pressure-longitudinal displacement relationship leads to the values of α_i , $i = 1, \dots, 6$ that approximate the following integer values:

$$(7.4) \quad \alpha_1 = 1, \quad \alpha_2 = 0, \quad \alpha_3 = 4, \quad \alpha_4 = 1, \quad \alpha_5 = -1, \quad \alpha_6 = -1.$$

The relative error is then obtained by comparing the data obtained using the FEM method and the data obtained using the values from Table 4 in formula (7.3). The relative errors are presented in Table 5.

TABLE 5

Relative errors for the least square method results presented in Table 4.

	relative ℓ^2 error N
$n_O = 6, n_L = 6$	4.5711×10^{-6}
$n_O = 8, n_L = 6$	3.649×10^{-6}
$n_O = 12, n_L = 6$	2.26763×10^{-6}

TABLE 6

Value for the parameters in formula (7.3) with u corresponding to the radial displacement.

	$\log k_r$	α_1	α_2	α_3	α_4	α_5	α_6
$n_O = 6, n_L = 6$	-0.578	0.987	0.012	3.940	1.053	-0.026	-1.972
$n_O = 8, n_L = 6$	-0.548	0.991	0.008	3.950	1.047	-0.016	-1.983
$n_O = 12, n_L = 6$	-0.527	0.997	0.002	3.978	1.024	-0.005	-1.994

TABLE 7

Relative error for the least square method results presented in Table 6.

	relative ℓ^2 error N
$n_O = 6, n_L = 6$	8.51638×10^{-6}
$n_O = 8, n_L = 6$	2.94811×10^{-6}
$n_O = 12, n_L = 6$	2.52609×10^{-6}

Similarly, for the pressure-radial displacement relationship the results of the least square method are presented in Table 6.

Based on those results we conclude the following.

CONCLUSION 3. The assumption (7.3) on the pressure-radial displacement relationship leads to the values of $\alpha_i, i = 1, \dots, 6$ that approximate the following integer values:

$$(7.5) \quad \alpha_1 = 1, \quad \alpha_2 = 0, \quad \alpha_3 = 4, \quad \alpha_4 = 1, \quad \alpha_5 = 0, \quad \alpha_6 = -2.$$

The ℓ^2 relative error for the results presented in Table 6 is shown in Table 7.

Based on the above results we obtain the following.

CONCLUSION 4. In the pressure-displacement relationship $p = Ku$, where u is either the radial displacement u_r in the middle of a stent or the longitudinal displacement u_l of the endpoints of a stent, the coefficient K depends on the Young's modulus of each strut E , on the width w and thickness t of each strut with rectangular cross section, and on the overall length L and reference radius R of the stent, via the following relationship:

- for the longitudinal displacement at the endpoints of a stent

$$(7.6) \quad p = \frac{k_l}{A^2} \frac{Ew^4t}{RL} u_l,$$

- for the radial displacement at the middle point of a stent

$$(7.7) \quad p = \frac{k_r}{A^2} \frac{Ew^4t}{L^2} u_r.$$

Here A is the total area of the struts, and k_l and k_r are the coefficients that depend on the number of vertices in the circumferential direction n_O and on the number of

TABLE 8

Parameters C , β_1 , and β_2 for the pressure-longitudinal displacement relationship.

	$\log C$	β_1	β_2	relative ℓ^2 error N
K	-4.434	2.046	2.022	0.000115332

TABLE 9

Parameters C , β_1 , and β_2 for the pressure-radial displacement relationship.

	$\log C$	β_1	β_2	relative ℓ^2 error N
K	-3.901	0.032	3.947	0.000161531

vertices in the longitudinal direction $n_L + 1$. The precise dependence of k_l and k_r on these parameters will be analyzed below.

Notice that formulas (7.6) and (7.7) differ by a factor of R/L . This is in agreement with the asymptotic expansions (with respect to R/L) leading to the rod equations which imply that the longitudinal displacement of a rod is by one order of magnitude smaller than the transverse displacement [9], namely,

$$(7.8) \quad u_l \approx \frac{R}{L} u_r.$$

Notice also that coefficient K does not depend on the shear modulus μ . This is to be expected, as noticed in Example 6.8, since the influence of the torsion of each cross section onto the overall pressure-displacement relationship of the stent should be of a lower order of magnitude, not captured in the leading-order behavior, using approximations (7.6) and (7.7).

In the last step of this procedure we determine how the coefficients k_l and k_r in formulas (7.6) and (7.7), respectively, depend on the geometrical parameters n_O and n_L . This will fully determine the dependence of K on the parameters in the problem. We make the following assumption:

$$p = \frac{C}{A^2} n_O^{\beta_1} n_L^{\beta_2} E^{\alpha_1} \mu^{\alpha_2} w^{\alpha_3} t^{\alpha_4} R^{\alpha_5} L^{\alpha_6} u,$$

where $\alpha_1, \dots, \alpha_6$ are given by either (7.4) or (7.5), depending on the considered case. Thus, we have assumed, in a similar fashion as before, that k_r and k_l depend on n_O and n_L through the powers β_1 and β_2 of n_O and n_L , respectively. The coefficient C and the powers β_i will depend on whether the longitudinal or the radial displacement is being considered. The results shown in Tables 8 and 9 show the values of the coefficients C , β_1 , and β_2 with the corresponding relative errors, calculated for the following sets of parameter values:

$$\begin{aligned} E &\in 2.1 \times 10^{11} \times \{0.8, 1, 1.2\}, & \mu &\in 8.31 \times 10^{10} \times \{0.85, 1, 1.15\}, \\ w &\in 0.0001 \times \{0.5, 1, 1.5\}, & t &\in 0.0001 \times \{0.5, 1, 1.5\}, \\ R &\in 0.01 \times \{0.8, 1, 1.2\}, & L &\in 0.018 \times \{0.8, 1, 1.2\}. \end{aligned}$$

CONCLUSION 5. The least square method indicates that the values of the parameters β_1 and β_2 are given by $\beta_1 = 0$, $\beta_2 = 4$ for the pressure-radial displacement relationship, and by $\beta_1 = 2$, $\beta_2 = 2$ for the pressure-longitudinal displacement relationship.

TABLE 10

Proportionality constant C_l for the longitudinal displacement of a stent at end points.

	$\log C_l$	relative $\frac{\ell^2}{N}$ error
K	-4.370	0.000172441

TABLE 11

Proportionality constant C_r for the radial displacement of a stent at the middle point.

	$\log C_r$	relative $\frac{\ell^2}{N}$ error
K	-3.916	0.00200469

Thus we have obtained the following.

Main result. Based on the data obtained using the finite element method simulations of the stent deformation under the uniform pressure applied to the interior or the exterior surface of a stent, the following simplified pressure-displacement relationship is obtained using the least square method approximation of the data for the longitudinal displacement at the endpoints of a stent u_l , and for the radial displacement of the middle point of a stent u_r :

$$(7.9) \quad p = C_l \frac{Ew^4 t n_O^2 n_L^2}{RLA^2} u_l = \frac{C_l}{4} \frac{Ew^2 t}{RLl_e^2} u_l,$$

$$(7.10) \quad p = C_r \frac{Ew^4 t n_L^4}{L^2 A^2} u_r = \frac{C_r}{4} \frac{Ew^2 t n_L^2}{L^2 l_e^2 n_O^2} u_r,$$

where

$$l_e^2 = 4R^2 \sin^2 \frac{\pi}{2n_0} + \left(\frac{L}{n_L} \right)^2.$$

Here E is the Young's modulus of the stent struts, w and t are the width and the thickness of the stent struts, R and L are the reference radius and length of the entire stent, n_O and $n_L + 1$ are the numbers of vertices in the circumferential and longitudinal directions, respectively, and

$$(7.11) \quad A = 2n_O n_L w l_e$$

is the area of the stent struts, where l_e is the distance of the endpoints of a strut (approximate strut length). Estimates for the values of the constants C_l and C_r , using the least square method, assuming the values of β_1 and β_2 as in Conclusion 5, are shown in Tables 10 and 11.

Derivation of the effective equations using the energy formulation. We can recover formulas (7.9) and (7.10) by studying the leading-order behavior of the energy of problem (4.8), obtained from its weak formulation assuming linear approximation of the curved stent struts.

Namely, the total energy of problem (4.8) is given by the following integral:

$$(7.12) \quad I_E := \frac{1}{2} \sum_{i,j,k} \int_0^{l_s} EI_n ((u_{i,j}^k)''_n)^2 + EI_b ((u_{i,j}^k)''_b)^2 + \mu K ((\tau_{i,j}^k)')^2 ds - \sum_{i,j,k} \int_0^{l_s} (f_{i,j}^k)_t (u_{i,j}^k)_t + (f_{i,j}^k)_n (u_{i,j}^k)_n + (f_{i,j}^k)_b (u_{i,j}^k)_b ds.$$

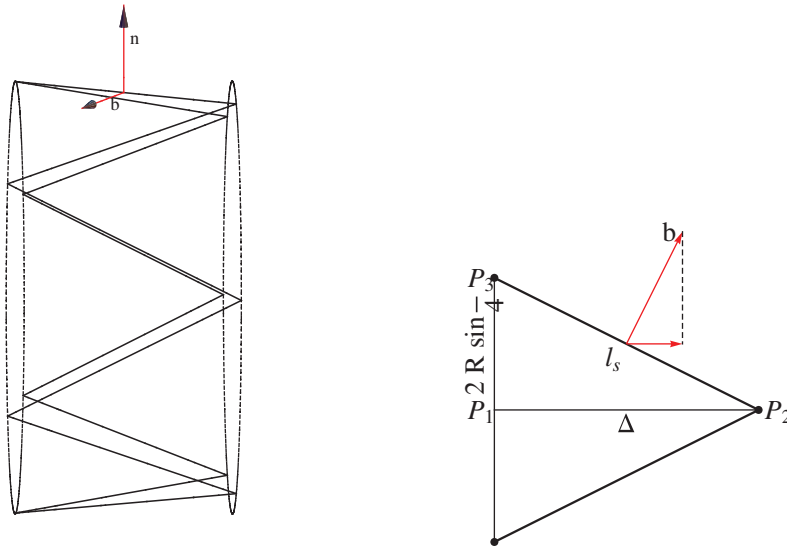


FIG. 22. Left: One circumferential ring of stent struts showing the normal (radial) and a bi-normal vector on one of the struts. Right: Right angle triangle P_1, P_2, P_3 with sides of length l_s (strut), Δ (parallel with the axis of symmetry), and $2R \sin(\phi/4)$ where ϕ is the angle defined in section 2, Figure 5.

The solution of problem (4.8)–(4.11) is the minimum of functional I_E given in (7.12) over the subspace determined by the conditions (4.9)–(4.11). In the energy integral (7.12) moments of inertia are given by

$$(7.13) \quad I_n = \frac{1}{12}wt^3 \quad \text{and} \quad I_b = \frac{1}{12}w^3t.$$

To study the leading-order behavior of (7.12), we introduce the nondimensional variables. To simplify notation, we first drop the i, j, k subscripts and superscripts and consider a generic straight rod whose displacement and torsion we denote by (u_t, u_n, u_b, τ) . Introduce the nondimensional variables $\bar{u}_t, \bar{u}_n, \bar{u}_b$, and $\bar{\tau}$ so that

$$(7.14) \quad \begin{aligned} u_t(l_s z) &= U_t \bar{u}_t(z), \\ u_n(l_s z) &= U_n \bar{u}_n(z), \\ u_b(l_s z) &= U_b \bar{u}_b(z), \\ \tau(l_s z) &= \bar{\tau}(z), \end{aligned}$$

which are defined on the unit interval $z \in (0, 1)$ where $s = l_s z$.

Consider one circumferential ring of struts as shown in Figure 22 left. Denote by U_l^{loc} the local (longitudinal) displacement of one circumferential ring of struts in the axial (longitudinal) direction. Assuming that each circumferential ring suffers the same local displacement U_l^{loc} , the total longitudinal displacement U_l of a stent consisting of n_L rings is given by $U_l = n_L U_L^{\text{loc}}$. From the right angle triangle P_1, P_2, P_3 shown in Figure 22 right, the bi-normal displacement U_b of a stent strut, the normal displacement U_n of a stent strut, and the local longitudinal displacement U_l^{loc} are related by the following:

$$(7.15) \quad U_b = \frac{l_s}{2R \sin(\phi/4)} U_l^{\text{loc}},$$

$$(7.16) \quad U_l^{\text{loc}} = \frac{R}{L} 4 \sin^2(\phi/4) n_L^2 U_n,$$

where ϕ is the angle defined in section 2, Figure 5. Equation (7.16) is obtained from the right angle triangle P_1, P_2, P_3 , shown in Figure 22 from which

$$\Delta^2 + 4R^2 \sin^2(\phi/4) = l_s^2.$$

Deformation of this triangle due to the negative local longitudinal displacement U_l^{loc} and positive normal (radial) displacement U_n (caused by the interior pressure loading) gives rise to

$$(\Delta - U_l^{\text{loc}})^2 + 4(R + U_n)^2 \sin^2(\phi/4) = l_s^2.$$

Here it was assumed that the right angle triangle is deformed (approximately) into another right angle triangle with sides $\Delta - U_l^{\text{loc}}$, $2(R + U_n) \sin(\phi/4)$, and l_s . Assuming U_n small, the first term in the Taylor series expansion of U_l^{loc} in terms of U_n is given by

$$U_l^{\text{loc}} = \frac{4R \sin^2(\phi/4)}{\sqrt{l_s^2 - 4R^2 \sin^2(\phi/4)}} U_n + \dots$$

Since the expression in the denominator equals Δ , we get

$$U_l^{\text{loc}} = \frac{4R \sin^2(\phi/4)}{\Delta} U_n + \dots$$

Finally, since $\Delta = L/n_L$ we recover (7.16). Thus, from the geometric considerations we have shown that the radial displacement corresponding to U_n and the longitudinal displacement U_l are related to the leading order via

$$(7.17) \quad U_l = \frac{R}{L} 4 \sin^2(\phi/4) n_L^2 U_n.$$

This can be simplified even further by noticing that the number of circumferential points in a stent n_O is typically greater than three, $n_O \geq 3$. Recalling that $\phi = 2\pi/n_O$ we see that $\phi/4 = \pi/(2n_O) \leq \pi/6$. Thus, the leading-order behavior of $\sin^2(\phi/4)$ is given by

$$(7.18) \quad \sin^2(\phi/4) = \frac{\pi^2}{4n_O^2} + \dots$$

Using this approximation we get that the leading-order relationship between U_l and U_n is given by

$$(7.19) \quad U_l = \frac{\pi^2}{n_O^2} \frac{R}{L} U_n.$$

This corresponds to the radial-longitudinal displacement relationship in terms of R/L , presented in formula (7.8).

We now turn back to the energy integral (7.12) to show that formulas (7.9) and (7.10) can be derived from (7.12) by taking into account only the term with the second-order derivative with respect to s of the *bi-normal component* of the displacement.

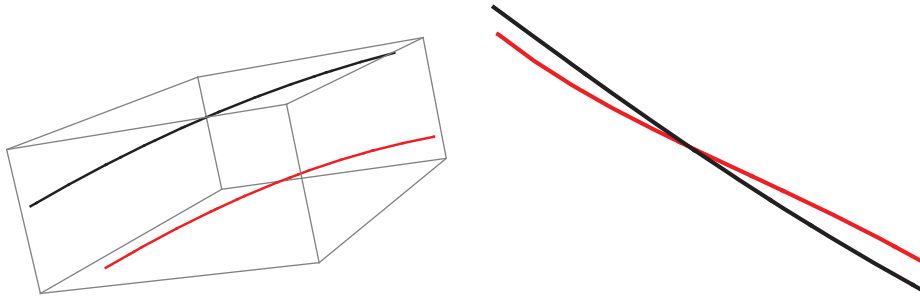


FIG. 23. Comparison between the reference strut (in black) and deformed strut (in red) viewed from the side (left picture) and from the top (right picture) indicating the normal displacement (left picture) and the bi-normal displacement (right picture).

This means that, to the leading order, the second-order derivative with respect to s of the normal displacement and the first-order derivative of the torsion of the strut's cross section are negligible with respect to the second-order derivative of the bi-normal displacement, under the uniform radial loading of a stent. This is reasonable. Namely, this means that the change in the curvature of a stent strut in the *bi-normal* direction is larger than the other contributions. Indeed, the most “visible” stent strut deformation is near the endpoints of a strut, at the vertices where the struts meet. This is, for example, visible in Figure 23 right where the curvature of the deformed strut, shown in red, is visibly different from the curvature of the undeformed strut, shown in black. The change in the strut curvature in the *normal* direction, shown in Figure 23 left is visibly smaller. Figure 23 left shows a comparison between a deformed strut, shown in red, and the reference strut, shown in black, viewed from the side (bi-normal direction) indicating the deformation of the strut in the *normal* direction.

Thus, we begin by calculating the term which contains u_b'' on the left-hand side of (7.12):

$$(7.20) \quad EI_b(u_b'')^2 = Etw^3 \left(U_b \frac{1}{l_s^2} \bar{u}_b'' \right)^2.$$

Now, by using (7.15) and (7.16) we obtain

$$U_b = 2l_s \sin(\phi/4) n_L \frac{1}{L} U_n.$$

By plugging this equation into (7.20) we get

$$(7.21) \quad EI_b(u_b'')^2 = \frac{Etw^3}{L^2 l_s^2} n_L^2 \sin^2(\phi/4) U_n^2 (\bar{u}_b'')^2.$$

We now take into account the right-hand side which incorporates the forcing in the normal direction which is given by the pressure p applied to the stent strut of width w , namely, pwU_n . By neglecting the lower order terms we conclude that coefficients of the leading-order terms should be proportional, with a nondimensional constant of proportionality C , namely,

$$(7.22) \quad p = C \frac{Etw^2}{L^2 l_s^2} n_L^2 \sin^2(\phi/4) U_n.$$

Now take into account that $A = 2n_0n_Lw_l_s$, as stated in (7.11), to obtain

$$(7.23) \quad p = C \frac{Etw^4}{L^2A^2} n_L^4 4n_0^2 \sin^2(\phi/4) U_n.$$

By taking into account the leading-order approximation of $\sin^2(\phi/4)$ given by (7.18), we get from (7.23) the following pressure-radial displacement relationship:

$$(7.24) \quad p = C \frac{Etw^4 n_L^4}{L^2A^2} U_n,$$

which is exactly formula (7.10).

By substituting (7.19) into (7.24) one obtains

$$(7.25) \quad p = C \frac{Etw^4 n_L^2 n_O^2}{LRA^2} U_l,$$

which is exactly formula (7.9).

REMARK 7.1. The fact that the leading-order energy behavior appears to be determined by the stent strut deformation in the bi-normal direction indicates that using the curved rod model, which captures stent strut deformation in all spatial directions, in contrast with a beam model, which captures deformation only in the direction of the forcing, provides a superior one-dimensional strut approximation over the conventional beam theory in the stent application at hand.

Consequences of formulas (7.10) and (7.9) can be summarized as follows.

COROLLARY 7.1. *In the production of a stent with uniform geometry, the radial stiffness of a stent increases with the higher Young's modulus and thickness of the stent struts, and with the width of the stent struts. The radial stiffness of a stent decreases with the larger reference length L . The precise dependence on all the parameters is given by formula (7.10).*

COROLLARY 7.2. *In the production of a stent with uniform geometry, the longitudinal stiffness of a stent increases with the higher Young's modulus and thickness of the stent struts and with the width of the stent struts. The longitudinal stiffness of a stent decreases with the increase in the total stent length L and with the increase of the reference radius R . The precise dependence on all the parameters is given by formula (7.9).*

Appendix A. In Example 6.1 we studied the behavior of a stent with reference radius 1 cm exposed to a uniform pressure load of 0.5 atm applied to the exterior surface of a stent, causing compression. The maximum radial displacement of the entire stent was assumed at the endpoints, and it was equal to 15% of the reference configuration. In this appendix we show that an arbitrary strut in this stent under this loading deforms much less than 15% and well within the realms of linear theory indicating that for the application discussed in this paper, using the linear theory of elasticity to describe the deformation of stent struts is appropriate. In order to do this we chose a strut which experiences maximal deformation in the sense of the contact moments (experiencing maximal loading). This is the strut with vertices $i = 5$ and $j = 13$ corresponding to one of the end struts. We calculated the total deformation of this strut. Figure 23 right shows a comparison between the reference configuration of the strut (shown in black) and the deformed strut (shown in red). The two are superimposed so that the deformed strut was translated to the position of the deformed strut in the least square sense. Figure 23 left shows the reference and the deformed

strut from the side (i.e., the bi-normal direction of the reference strut). The maximal displacement of the strut divided by the strut length was calculated to be equal to 6.5% which is well within the realms of linear theory. This indicates the appropriateness of the use of linear theory to study compression and expansion of an already expanded stent under the physiologically relevant cyclic loading of approximately 0.5 atm.

Appendix B. To compare the performance between the 1D curved rod model employed in this manuscript to describe the mechanical properties of stent struts, with a 3D finite element method approximation of a curved rod using 3D linear elasticity, we consider here a semicircular rod of radius 8×10^{-4} m (middle curve radius), and with a square cross section of thickness 2.5×10^{-5} m; see Figure 24. The semicircular rod with these dimensions has approximately the same aspect ratio as the stent struts considered in Example 6.1 of this manuscript. Namely, the aspect ratio of the semicircular rod is

$$\epsilon = \frac{w}{l_s} = \frac{2.5 \times 10^{-5}}{\pi \times 8 \times 10^{-4}} = 0.1 \times 10^{-1} = 10^{-2},$$

while the aspect ratio for the struts of the stent considered in Example 6.1 is $\epsilon_{(\text{Ex1})} = 1.6 \times 10^{-2}$ m. (In [9] it was shown mathematically that the 1D curved rod model approximates the 3D problem in the sense that the 3D displacement converges to the solution of the 1D problem in the H^1 sense as the aspect ratio $\epsilon \rightarrow 0$.)

The semicircular rod considered in this appendix was exposed to the loading of a force with two components different from zero:

$$\mathbf{f} = (f_x, f_y, f_z) = (0, 10^9, -10^{11})N/m^3,$$

where the y -direction, as shown in Figure 24, points toward the viewer, and the negative z -direction points downward. The rod was fixed at the endpoints with a square basis assuming the homogeneous Dirichlet boundary conditions.

A three-dimensional FEM approximation of the rod was performed using `freefem3d` (<http://www.freefem.org/ff3d/>) with 344259 tetrahedral elements. This gave rise to a system matrix of dimension 217017. The same problem was solved using a FEM approximation of the 1D curved rod model, presented in this manuscript, with 100 discretization points along the middle curve of the rod giving rise to a system matrix of dimension 606. Figures 24 and 25 show a comparison between the 3D (left) and 1D (right) approximations of the deformations of the rod. The pictures are colored based on the magnitude of the y component of the displacement. The difference between the two approximations is 0.5% of the displacement with the maximum y displacement

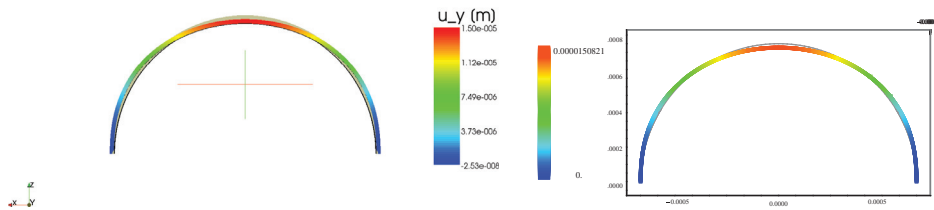


FIG. 24. The 3D (left) and 1D (right) simulations of a curved rod deformation. The reference configuration is shown in grey. The rod is colored based on the magnitude of the y component of the displacement. The difference between the two calculations is less than $8 \times \epsilon^{-4}$ where $\epsilon = 10^{-2}$ is the aspect ratio of the rod.

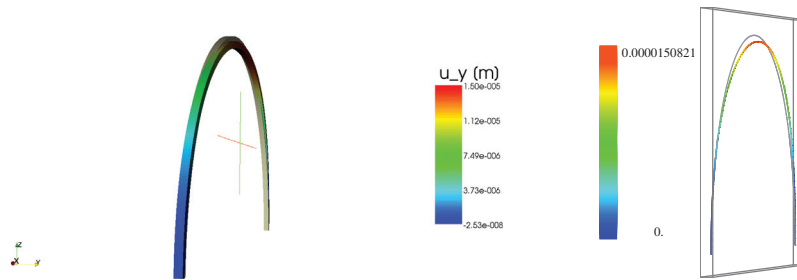


FIG. 25. Side view of the semicircular rod shown in Figure 24.

equal to 1.5×10^{-5} m. This is of order $8 \times \epsilon^4$ where $\epsilon = 10^{-2}$ is the aspect ratio of the rod. The difference in the other two components of the displacement were less than or equal to the reported error of the y -displacement, thereby indicating excellent approximation by the 1D curved rod model at a much smaller computational cost.

REFERENCES

- [1] S. S. ANTMAN, *Nonlinear Problems of Elasticity*, Springer, New York, 2005.
- [2] J. L. BERRY, A. SANTAMARINA, J. E. MOORE, JR., S. ROYCHOWDHURY, AND W. D. ROUTH, *Experimental and computational flow evaluation of coronary stents*, *Ann. Biomed. Engng.*, 28 (2000), pp. 386–398.
- [3] S. ČANIĆ, C. J. HARTLEY, D. ROSENSTRAUCH, J. TAMBAČA, G. GUIDOBONI, AND A. MIKELIĆ, *Blood flow in compliant arteries: An effective viscoelastic reduced model, numerics and experimental validation*, *Ann. Biomed. Engng.*, 34 (2006), pp. 575–592.
- [4] P. G. CIARLET, *Mathematical Elasticity. Volume I: Three-Dimensional Elasticity*, North-Holland, Amsterdam, 1988.
- [5] C. DUMOULIN AND B. COCHELIN, *Mechanical behaviour modelling of balloon-expandable stents*, *J. Biomechanics*, 33 (2000), pp. 1461–1470.
- [6] A. O. FRANK, P. W. WALSH, AND J. E. MOORE, JR., *Computational fluid dynamics and stent design*, *Artificial Organs*, 26 (2002), pp. 614–621.
- [7] Y. C. FUNG, *Biomechanics: Mechanical Properties of Living Tissues*, 2nd ed., Springer, New York, 1993.
- [8] G. HAUSDORF, *Mechanical and biophysical aspects of stents*, in *Catheter Based Devices for the Treatment of Non-coronary Cardiovascular Diseases in Adults and Children*, P. S. Rao and M. J. Kern, eds., Lippincott Williams & Wilkins, Philadelphia, 2003, pp. 271–285.
- [9] M. JURAK AND J. TAMBAČA, *Derivation and justification of a curved rod model*, *Math. Models Methods Appl. Sci.*, 9 (1999), pp. 991–1014.
- [10] M. JURAK AND J. TAMBAČA, *Linear curved rod model. General curve*, *Math. Models Methods Appl. Sci.*, 11 (2001), pp. 1237–1252.
- [11] K. W. LAU, A. JOHAN, U. SIGWART, AND J. S. HUNG, *A stent is not just a stent: Stent construction and design do matter in its clinical performance*, *Singapore Med. J.*, 45 (2004), pp. 305–312.
- [12] D. R. McCLEAN AND N. EIGLER, *Stent Design: Implications for Restenosis*, MedReviews, LLC, New York, 2002.
- [13] F. MIGLIAVACCA, L. PETRINI, M. COLOMBO, F. AURICCHIO, AND R. PIETRABISSA, *Mechanical behavior of coronary stents investigated through the finite element method*, *J. Biomechanics*, 35 (2002), pp. 803–811.
- [14] J. E. MOORE, JR., AND J. L. BERRY, *Fluid and solid mechanical implications of vascular stenting*, *Ann. Biomed. Engng.*, 30 (2002), pp. 498–508.
- [15] A. C. MORTON, D. CROSSMAN, AND J. GUNN, *The influence of physical stent parameters upon restenosis*, *Pathologie Biologie*, 52 (2004), pp. 196–205.
- [16] D. PANIAGUA, E. INDUNI, C. ORTIZ, C. MEJIA, F. LOPEZ-JIMENEZ, AND R. D. FISH, *Images in cardiovascular medicine. Percutaneous heart valve in the chronic in vitro testing model*, *Circulation*, 106 (2002), pp. e51–52.

- [17] D. PANIAGUA, J. A. CONDADO, J. BESSO, M. VÉLEZ, B. BURGER, S. BIBBO, D. CEDENO, H. ACQUATELLA, C. MEJIA, E. INDUNI, AND R. D. FISH, *First human case of retrograde transcatheter implantation of an aortic valve prosthesis*, Texas Heart Inst. J., 32 (2005), pp. 393–398.
- [18] J. TAMBAČA, *A model of irregular curved rods*, in Proceedings of the Conference on Applied Mathematics and Scientific Computing, Dubrovnik, 2001, Z. Drmač, V. Hari, L. Sopta, Z. Tutek, K. Veselić, eds., Kluwer, Dordrecht, 2003, pp. 289–299.
- [19] J. TAMBAČA, *A numerical method for solving the curved rod model*, ZAMM, 86 (2006), pp. 210–221.
- [20] J. TAMBAČA, S. ČANIĆ, AND D. PANIAGUA, *Mechanical Behavior of Fully Expanded Commercially Available Endovascular Coronary Stents in the US*, submitted.
- [21] L. H. TIMMINS, M. R. MORENO, C. A. MEYER, J. C. CRISCIONE, A. RACHEV, AND J. E. MOORE, JR., *Stented artery biomechanics and device design optimization*, Med. Bio. Eng. Comput, 45 (2007), pp. 505–513.